Behavioral Characteristics, Associative Learning Capabilities, and Dynamic Association Mapping in an Animal Model of Cerebellar Degeneration

Elena Porras-García, Raudel Sánchez-Campusano, David Martínez-Vargas, Eduardo Domínguez-del-Toro, Jan Cendelín, Frantisek Vozeh and José M. Delgado-García

J Neurophysiol 104:346-365, 2010. First published 21 April 2010; doi:10.1152/jn.00180.2010

J Neurophysiol 104: 346–365, 2010.
First published April 21, 2010; doi:10.1152/jn.00180.2010.

Behavioral Characteristics, Associative Learning Capabilities, and Dynamic Association Mapping in an Animal Model of Cerebellar Degeneration

Elena Porras-García,[1,2,*] Raudel Sánchez-Campusano,[2,*] David Martínez-Vargas,[3] Eduardo Domínguez-del-Toro,[2] Jan Cendelín,[4] František Vožeh,[4] and José M. Delgado-García[2]

[1]*Division of Anatomy and Human Embryology and* [2]*Division of Neurosciences, Pablo de Olavide University, Seville, Spain;* [3]*Dirección de Investigaciones en Neurociencias, Instituto Nacional de Psiquiatría Ramón de la Fuente Muñiz, San Lorenzo Huipulco, Mexico City, Mexico; and* [4]*Department of Pathophysiology, Faculty of Medicine in Pilsen, Charles University, Pilsen, Czech Republic*

Submitted 16 February 2010; accepted in final form 21 April 2010

Porras-García E, Sánchez-Campusano R, Martínez-Vargas D, Domínguez-del-Toro E, Cendelín J, Vožeh F, Delgado-García JM. Behavioral characteristics, associative learning capabilities, and dynamic association mapping in an animal model of cerebellar degeneration. *J Neurophysiol* 104: 346–365, 2010. First published April 21, 2010; doi:10.1152/jn.00180.2010. Young adult heterozygous Lurcher mice constitute an excellent model for studying the role of the cerebellar cortex in motor performance—including the acquisition of new motor abilities—because of the early postnatal degeneration of almost all of their Purkinje and granular cells. Wild-type and Lurcher mice were classically conditioned for eyelid responses using a delay paradigm with or without an electrolytic lesion in the interpositus nucleus. Although the late component of electrically evoked blink reflexes was smaller in amplitude and had a longer latency in Lurcher mice than that in controls, the two groups of animals presented similar acquisition curves for eyeblink conditioning. The lesion of the interpositus nucleus affected both groups of animals equally for the generation of reflex and conditioned eyelid responses. Furthermore, we recorded the multiunitary activity at the red and interpositus nuclei during the same type of associative learning. In both nuclei, the neural firing activity lagged the beginning of the conditioned response (determined by orbicularis oculi muscle response). Although red nucleus neurons and muscle activities presented a clear functional coupling (strong correlation and low asymmetry) across conditioning, the coupling between interpositus neurons and either red nucleus neurons or muscle activities was slightly significant (weak correlation and high asymmetry). Lurcher mice presented a nonlinear coupling (high asymmetry) between red nucleus neurons and muscle activities, with an evident compensatory adjustment in the correlation of firing between interpositus and red nuclei neurons (a coupling with low asymmetry), aimed probably at compensating the absence of cerebellar cortical neurons.

INTRODUCTION

The role of cerebellar circuits in the acquisition of new motor abilities and, in particular, in the classical conditioning of eyelid responses has been studied and analyzed repeatedly in the past three decades using different experimental approaches, ranging from transient or permanent lesions of cerebellar structures in rabbits and cats (Bracha et al. 1999; Christian and Thompson 2003; Jiménez-Díaz et al. 2004; Yeo et al. 1985) to electrophysiological recordings from cerebellar cortical and nuclear neurons (Gruart et al. 2000) and by the use of mutant or genetically manipulated mice (Chen et al. 1996; Kishimoto et al. 2001, 2002; Koekkoek et al. 2003, 2005; Porras-García et al. 2005). Nevertheless, it still seems necessary not only to determine the specific role of cerebellar cortical and nuclear structures in the same experimental model, but also to record the neural activity of the interpositus–red nucleus pathway during the acquisition process.

In a first series of experiments, we attempted to determine the role of cerebellar cortical and nuclear areas in the acquisition of this type of associative learning, combining the use of wild-type and Lurcher mice with the electrolytic lesion of the interpositus nucleus. Lurcher mutants carry a spontaneous mutation in a gene coding for the GluRδ2 receptor, constituting a good model of cerebellar decortication, because adult individuals have no Purkinje cells (Caddy and Biscoe 1979; Cendelín et al. 2008, 2009; Porras-García et al. 2005; Vogel et al. 2007; Yuzaki 2004; Zuo et al. 1997). In the present study, we carried out the classical conditioning of eyelid responses with a delay paradigm in interpositus-lesioned and -nonlesioned wild-type and Lurcher mice. Conditioned responses were determined from the electromyographic (EMG) activity of the orbicularis oculi (OO) muscle.

For a better understanding of the information processing at different levels of the motor system and, in particular, the functional mapping of the dynamic associations between electrophysiological signals recorded during actual motor learning processes, a directional analysis to reveal the strength (strong or weak), the type (linear or symmetric, nonlinear or asymmetric), the temporal order (time delays between the signals), and the functional nature (unidirectional or bidirectional) of couplings in the interpositus nucleus–red nucleus–final motor pathway network seems to be essential. This strategy (i.e., dynamic association mapping) integrates mathematical relationships (i.e., a directional analysis determined by the nonlinear correlation method) of different traits or variables (i.e., electrophysiological recordings and their parameters) in different cerebral sites (i.e., cerebellar, premotor, and motor areas) within the brain mapping framework. The nonlinear correlation method (Ansari-Asl et al. 2006; Kalitzin et al. 2007; Lopes da Silva et al. 1989; Meeren et al. 2002; Pereda et al. 2005; Pijn et al. 1997; Wendling et al. 2001) have proven useful in these experimental situations (Bernasconi et al. 2000; Kamiński and Liang 2005; Sánchez-Campusano et al. 2009; Witte et al. 2009).

Accordingly, in a second series of experiments, we carried out a nonlinear correlation analysis to quantify the dynamic associations or functional couplings (the correlation code and

* These authors contributed equally to this work.

Address for reprint requests and other correspondence: J. M. Delgado-García, División de Neurociencias, Universidad Pablo de Olavide, Ctra. de Utrera, Km. 1, Sevilla-41013, Spain (E-mail: jmdelgar@upo.es).

the temporal order) present in the multiunitary activity (MUA) of neurons recorded simultaneously from the red and the interpositus nuclei and the EMG activity of the OO muscle, as an output signal. The correlation code (the strength and type of interdependence between signals, including the asymmetry information) and the temporal order (time delay in coupling) were used to assess a directional analysis with causal inferences during the learning process. The aim was to determine the causal involvement of the interpositus nucleus and its immediate target, the red nucleus, in the generation of new motor abilities, using as an experimental model the classical conditioning of eyelid responses in wild-type and Lurcher mice.

METHODS

Subjects

Experiments were carried out on male wild-type and Lurcher mutant mice in a B6CBA background. Mice were obtained from the Medical Faculty Animal House of Charles University (Pilsen, Czech Republic) and came from the same litters. Animals were 3–5 mo old, weighing 24–30 g, on arrival. Before surgery, animals were housed in separate cages ($n = 10$ per cage) and kept on a 12-h light/12-h dark cycle with constant ambient temperature (22 ± 1°C) and humidity (60 ± 5%). Food and water were available without restriction. After surgery, animals were kept in individual cages. Experiments were finished in the 3 mo following the animals' arrival. Electrophysiological and behavioral studies were performed in accordance with the guidelines of the European Union Council (2003/65/EU) and current Spanish regulations (BOE 252/34367-91 2005) for the use of laboratory animals in chronic experiments. Experiments were also approved by the Ethics Committee of the Pablo de Olavide University for animal care and handling.

Surgical procedures

For the first series of experiments (lesion of the interpositus nucleus, Figs. 1–5), both wild-type and Lurcher mice were divided in three groups ($n = 8$ each): lesioned, sham, and controls. Animals were anesthetized with a mixture of ketamine (100 mg/kg) and xylazine (20 mg/kg). Once anesthetized, stereotaxic coordinates (Paxinos and Franklin 2001) were followed to implant animals with bipolar stimulating electrodes aimed at the left interpositus nucleus (1.4 mm lateral and 6.4 mm posterior to bregma; depth from brain surface: 2.3 mm for wild-type and 1–1.2 mm for Lurcher mice). These electrodes were made of 50 μm, Teflon-coated tungsten wires (Advent Research Materials, Eynsham, UK). For the lesion of the interpositus nucleus, an anodic current (1.5 mA) was applied for 10 s (Fig. 1). In sham animals, electrodes were also implanted in the interpositus nucleus, but no electric current was injected across them. Afterward, stimulant electrodes were removed and the cranial hole was filled with sterile bone wax. During the same surgical step, animals were also implanted with bipolar stimulating electrodes on the left (ipsilateral) supraorbital nerve and with bipolar recording electrodes in the ipsilateral OO muscle. These electrodes were made of 50 μm, Teflon-coated, annealed stainless steel wire (A-M Systems, Carlsborg, WA), with their tips bared of the isolating cover for about 0.5 mm. Electrode tips were bent as a hook to facilitate a stable insertion in the upper eyelid. Control animals were implanted only with eyelid recording and stimulating electrodes. The wires were soldered to a four-pin socket (RS-Amidata, Madrid), which was fixed to the skull with the help of two small screws and dental cement. Finally, the skin overlying the cranium was stitched up around the sockets (Domínguez-del-Toro et al. 2004).

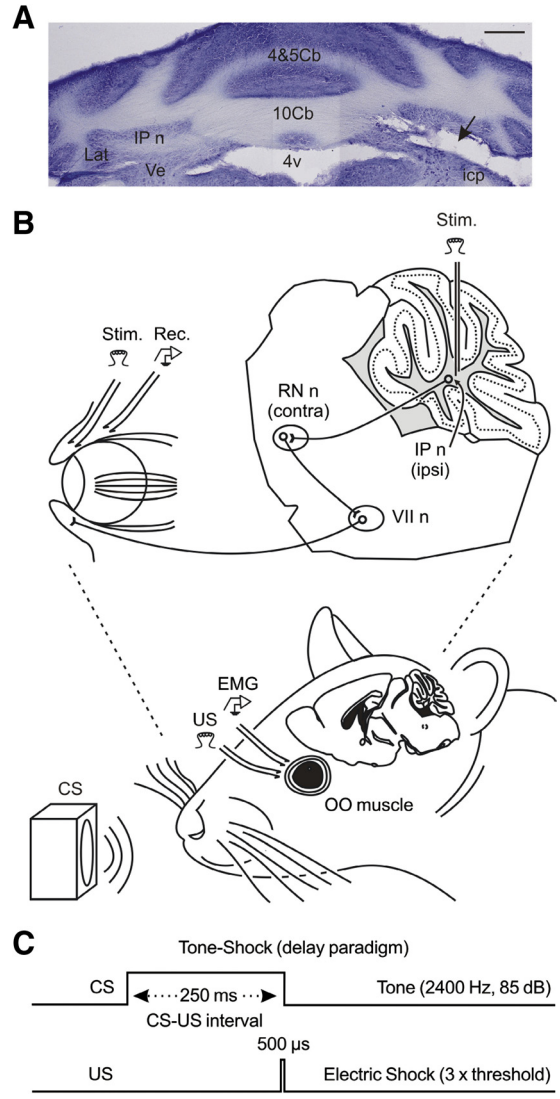

FIG. 1. Classical conditioning of eyelid responses in wild-type and Lurcher mice with or without a lesion of the cerebellar interpositus nucleus. *A*: photomicrography of a Nissl staining illustrating the location of the lesion (arrow) produced in the interpositus (IP) nucleus in a wild-type mouse. Calibration bar = 500 μm. *B*: experimental design. The left interpositus nucleus (IP n) was lesioned with anodic current (1.5 mA for 10 s). Animals were chronically implanted with electromyographic (EMG) recording electrodes in the upper part of the left orbicularis oculi (OO) muscle. Bipolar stimulating electrodes were implanted on the left supraorbital nerve for unconditioned stimulus (US) presentation. *C*: for classical conditioning of eyelid responses, we used a delay paradigm consisting of a tone (250 ms, 2.4 kHz, 85 dB) as the conditioned stimulus (CS). The CS started 249.5 ms before and coterminated with the electric shock (500 μs, 3 × threshold) used as US. icp, inferior cerebellar peduncle; Lat, dentate cerebellar nucleus; Ve, vestibular nucleus; VII n, facial nucleus; 4&5Cb, 4th and 5th cerebellar lobules; 4V, 4th ventricle; 10Cb, 10th cerebellar lobule; Stim., stimulating sites; Rec., recording sites.

In the second series of experiments, animals (wild-type and Lurcher mice; $n = 8$ per group) were prepared for electrophysiological recordings from red and interpositus nuclei neurons during the classical conditioning of eyelid responses (Figs. 6–12). Mice were anesthetized as described earlier. Once anesthetized, stereotaxic coordinates (Paxinos and Franklin 2001) were followed to implant animals with bipolar recording and stimulating electrodes aimed at the right (contralateral) red nucleus (0.7 mm lateral and 3.5 mm posterior to bregma; depth from brain surface: 3.5 mm) and at the left (ipsilateral)

interpositus nucleus (1.4 mm lateral and 6.4 mm posterior to bregma; depth from brain surface: 2.3 mm for wild-type and 1–1.2 mm for Lurcher mice; Fig. 6 and Supplemental Fig. S2).[1] The final location of red-nucleus electrodes was adjusted to evoke a contralateral eyeblink following the presentation of a single cathodic (500 μs, 0.5 mA) pulse, whereas the final location of the electrodes implanted in the interpositus nucleus was adjusted with the help of the antidromic field potential evoked in this nucleus by pairs of pulses (cathodic, 500 μs, $<$0.6 mA, 5- to 200-ms interval) presented to the contralateral red nucleus (see Fig. 2 and Gruart and Delgado-García 1994 for details). These electrodes were made of 25–50 μm, Teflon-coated tungsten wires (Advent Research Materials). Animals were also implanted with bipolar stimulating electrodes on the left supraorbital nerve and with bipolar recording electrodes in the ipsilateral OO muscle. Palpebral electrodes were made of 50 μm, Teflon-coated, annealed stainless steel wire (A-M Systems), with their tips bared of the isolating cover for about 0.5 mm. A 0.1 mm bare silver wire was affixed to the skull as ground. The eight wires and the ground were connected to two (four-pin and six-pin) sockets (RS-Amidata), each of which was fixed to the skull with the help of two small screws and dental cement (Domínguez-del-Toro et al. 2004).

Three additional control animals were prepared for recording eyelid movements with the magnetic search-coil technique (CNC Engineering, Seattle, WA). A 30-turn coil made of enamel-insulated 25-μm copper wire, 1-mm OD was implanted in the upper eyelid following procedures described elsewhere (Gruart et al. 1995). Coils were calibrated by rotating the magnetic field frame $\pm$20° in the vertical plane with the mouse still under the effects of the anesthetic. The gain of the recording system was adjusted to yield 1 V per 20°. Eyelid maximum opening was about 40° for the three animals. These three animals were also implanted with OO EMG recording electrodes in the contralateral eyelid and with stimulating electrodes aimed to activate the supraorbital nerve bilaterally (see Fig. 3*F* and Supplemental Fig. S1).

Classical conditioning of eyelid responses

For conditioning, the animal was placed in a small (5 $\times$ 5 $\times$ 10 cm) plastic chamber located inside a larger Faraday box. A small hole in the chamber top allowed the passage of the four-strand and six-strand cables connecting the animal to the recording and stimulating system. Classical conditioning was achieved using a delay paradigm (Fig. 1*C*). For this, a tone (2,400 Hz, 85 dB, 250 ms) was presented as a conditioned stimulus (CS). The unconditioned stimulus (US) consisted of a long (500 μs), strong (3 $\times$ threshold), square, cathodal pulse. Intensities for the US ranged from 0.2 to 0.5 mA. Both CS and US ended simultaneously. Electrical stimulation was carried out with the help of a CS-20 stimulator across an isolation unit (Cibertec, Madrid).

For the first series of experiments (lesion of the interpositus nucleus), each animal underwent three habituation, nine conditioning, and four extinction sessions. A conditioning session consisted of the paired CS–US presentation for 60 times at intervals of 30 $\pm$ 5 s. The session lasted roughly 30 min. For habituation and extinction sessions, only the CS was presented, also 60 times per session and at intervals of 30 $\pm$ 5 s. The large number of habituation sessions carried out in this study was aimed to reduce as much as possible the incidence of alpha responses (see Fig. 3; Domínguez-del-Toro et al. 2004).

For the second series of experiments (electrophysiological recordings of red and interpositus nuclei neurons during the classical conditioning of eyelid responses), each animal underwent three habituation and nine conditioning sessions. In this experiment, a conditioning session consisted of the paired CS–US presentation for 100 times at intervals of 30 $\pm$ 5 s. In this case, conditioning sessions lasted close to 50 min. For habituation sessions, only the CS was presented, also 100 times per session and at intervals of 30 $\pm$ 5 s.

In both experiments, the CS was presented alone in 10% of the cases to enable a proper analysis of evoked conditioned responses.

Recording and stimulating techniques

The EMG activity of the OO muscle and the neuronal MUA of both red and interpositus nuclei were recorded using three Grass P511 differential amplifiers with a bandwidth ranging from 1 Hz to 10 kHz (Grass-Telefactor, West Warwick, RI).

Reflex blinks were evoked by single 50-μs, 2 $\times$ threshold, square, cathodal pulses presented at a rate of 1/30 s. Reflex blink responses were collected before the initiation of the conditioning sessions from lesioned and nonlesioned wild-type and Lurcher mice.

As a criterion, we considered a "conditioned response" as the presence during the CS–US period of EMG activity in the OO muscle that lasted $>$20 ms and was initiated $>$50 ms after CS onset. In addition, the integrated EMG activity recorded during the CS–US interval had to be $\geq$1.5-fold larger than the averaged activity recorded immediately before CS presentation. The percentage of conditioned

[1] The online version of this article contains supplemental data.

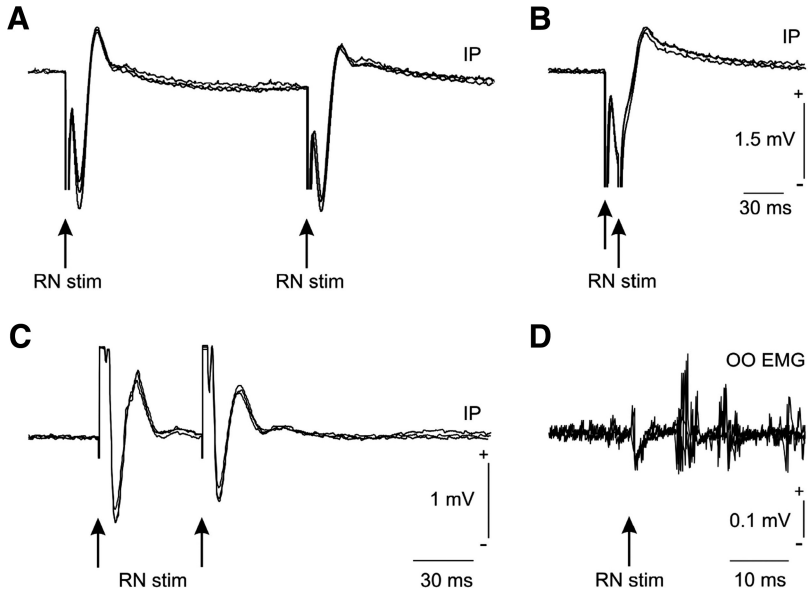

FIG. 2. Antidromic field potentials recorded in the interpositus nucleus following red nucleus stimulation in a wild-type mouse. *A*: illustrations of 3 superimposed field potentials evoked in the interpositus nucleus following paired-pulse stimulation (500 μs, 0.2 mA, 170 ms interval) of the red nucleus. Note that the 2 antidromic field potentials presented similar amplitudes. However, when the interval was reduced to 10 ms, the 2nd pulse did not evoke any field (*B*). *C*: illustration of the effect on the 2nd field potential of an interval of 75 ms. *D*: 3 superimposed EMG traces recorded from the OO muscle of a wild-type animal following stimulation (500 μs, 0.5 mA) of the contralateral red nucleus.

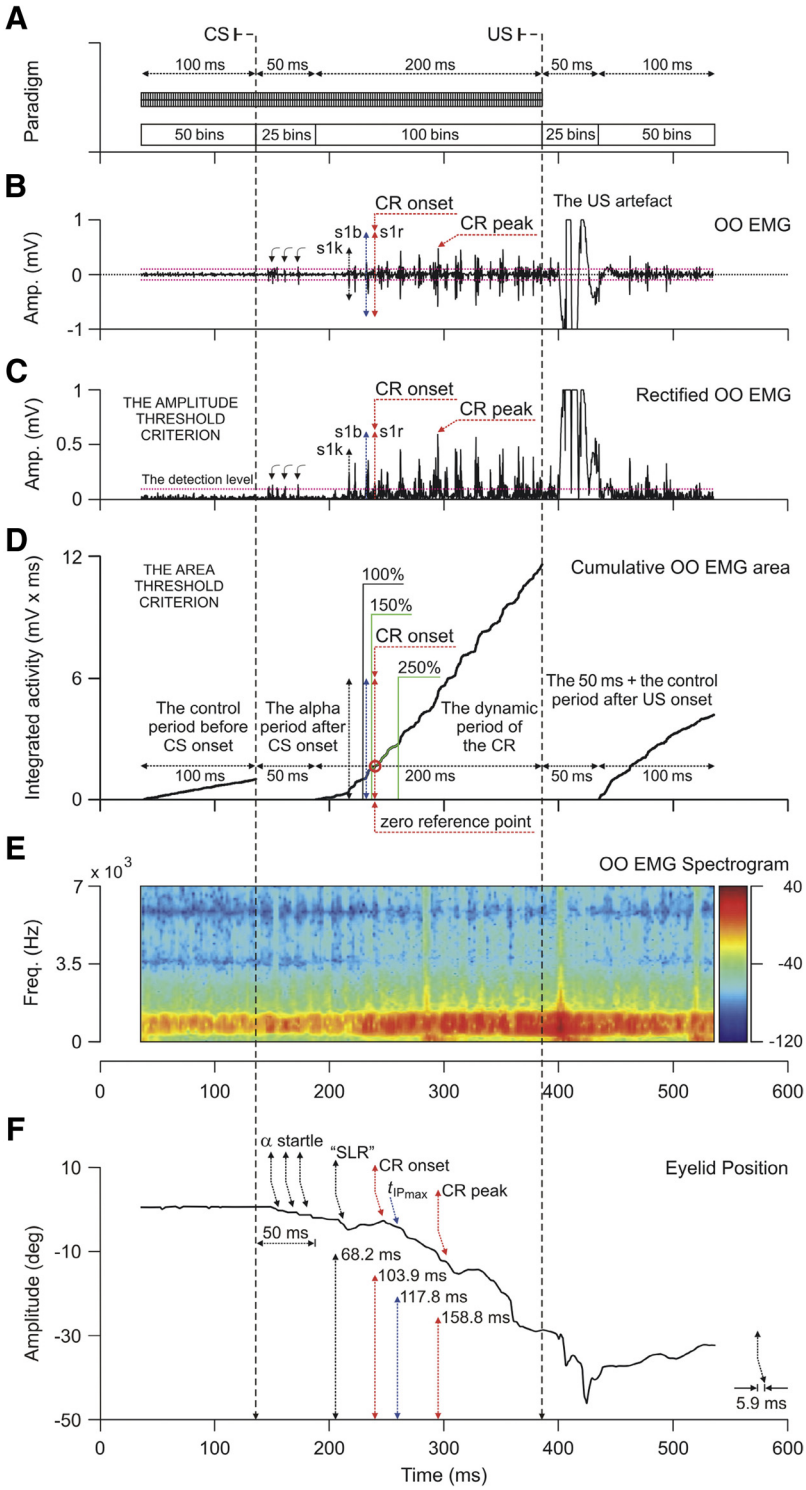

FIG. 3. Quantitative EMG analysis and determination of the onset of conditioned responses (CRs). *A–C*: the rectified and averaged (n = 10 trials) EMG recording from the 9th (C9) conditioning session of a wild-type mouse is illustrated. This rectified OO EMG recording (*B*) ranged from 100 ms before CS initiation to 150 ms after US presentation. Magenta horizontal dashed lines indicate the detection levels (mean of the first 50 bins + 5SD). Curved arrows indicate the appearance of alpha responses to tone (CS) presentation in the first 50 ms after CS onset. The 1st spikes that overcome the detection level in the different statistical ranges of thresholds areas (s1k spike in black, for >50% with a latency of 80.33 ms; s1b spike in blue, for >100% with a latency of 96.29 ms; s1r in red, for >150% with a latency of 103.92 ms after CS onset) are indicated with the color arrows. *D*: the evolution of the cumulative integrated EMG activity (in mV · ms) in the control (100 ms prior to CS onset) and dynamic (250 ms after CS onset) periods of the CR is also shown. The red arrows show the latencies to onset (103.92 ms) and peak (158.75 ms) of the CR as determined by computer software optimizing the amplitude threshold and cumulative area threshold statistic criteria (see Supplemental APPENDIX S1). The start of the CR is taken as the zero reference point of the dynamic correlation range. *E*: the time–frequency representation of the OO EMG activity is also illustrated with a predominant frequency range of 500–1,500 Hz in the entire time window. *F*: averaged (n = 10 trials) eyelid responses collected from the same animal. Note that eyelid movements followed (with a delay of 5.9 ms, as indicated by the curved arrows) the EMG activity of the OO muscle. Times corresponding to alpha responses (α startle), CR onset and peak, and t_{IPmax} are indicated. For the sake of comparison, the latency for the "SLR" responses (Boele et al. 2010) is also indicated. The eye of the mouse is open at 0° and totally closed at 40°, i.e., at amplitude = 0 mm the eyelid is maximum opened, at 1 mm the eyelid is fully closed, also in agreement with the above-mentioned article.

responses (% CRs) was determined from the number of CS presentations that elicited a conditioned response reaching the indicated criteria. In accordance with previous descriptions (Boele et al. 2010; Domínguez-del-Toro et al. 2004; Koekkoek et al. 2002; Porras-García et al. 2005; Svensson et al. 1997), the selected criteria included the analysis of the amplitude and area of evoked eyelid responses as determined by quantitative analysis of the EMG activity of the OO muscle (see Fig. 3 for details). Refer to Supplemental APPENDIX S1 for a detailed and practical description of the cumulative integrated method for the quantitative EMG analysis.

Histology

At the end of the experiments, animals were deeply anesthetized (sodium pentobarbital, 50 mg/kg, administered intraperitoneally) and perfused transcardially with saline and 4% phosphate-buffered paraformaldehyde. Serial sections (50 μm) including the brain stem and the cerebellum were mounted on gelatinized glass slides and stained using the Nissl technique with 0.1% toluidine blue, to confirm not only the location of the stimulating and/or recording electrodes, but also the extent of the evoked electrolytic lesions (see Figs. 1*A* and 6*A* and Supplemental Fig. S2).

Data collection and analysis

The EMG of the OO muscle, MUA recorded in red and interpositus nuclei, and rectangular pulses corresponding to CS and US presentations were stored digitally on a computer, using an analog–digital converter (CED 1401 Plus; Ceta Electronic Design, Cambridge, UK). Commercial computer programs (Spike2 and SIGAVG; Ceta Electronic Design) were used for acquisition and on-line conventional analysis. The multivariate off-line analyses of electrophysiological signals, the analytical procedures (including spike detection, phase space reconstruction, and multiparametric cluster techniques), and the representation programs used for data illustrated in Figs. 3 and 8–12, in the main text, and Supplemental Figs. S1, S3, and S4 were developed by one of us (R.S.-C.) with the help of MATLAB routines (The MathWorks, Natick, MA). Only successful animals (i.e., those that allowed a complete study with an appropriate functioning of both recording and stimulating systems) were computed and analyzed.

Multiunitary raw activities recorded from red nucleus and interpositus neurons were computed and quantified. The quantification algorithm also took into account the identification of the activity's standard waveform and the classification of probability patterns of spikes in time and frequency domains (Brown et al. 2004; Jarvis and Mitra 2001; Sánchez-Campusano et al. 2007) and in the phase space (Aksenova et al. 2003; Chan et al. 2008). Since multiunitary neuronal recordings usually contain overlapping spikes, we selected the following analytical procedure. Using a spike-sorting method, overlapping spikes within an interval of 1 ms were regarded as a single spike (according to the absolute refractory period) and overlapping spikes within an interval of 1–3 ms were regarded as spikes of different classes due to the interspike interval (i.e., the relative refractory period of the neuron) criterion in spike detection.

Thus we applied the spike-pattern classification method, including the preliminary time–frequency analyses, the multivariate cluster techniques, the overlapped spikes resolution, the amplitude thresholds, the absolute and relative refractory periods, and the typical waveform (in time domain and in the phase space) criteria in spike detection. The time–frequency spectrogram was used to show the frequency band of pure electrophysiological signal components. We were able to do this because the spectrograms contain an estimate of the short-term, time-localized frequency content of the signals (MUA recordings and OO EMG activity). The cluster tools enabled us to determine the numbers of cells, classes, and spikes and their centers by measuring the distances between their trajectories in phase space. Spike phase space reconstruction was implemented using the time delay technique and the reconstructed spike waveform (an ideal and undisturbed spike that can be used as a template for the sorting method) preserves essential characteristics and the major phase space trajectory of the original spike.

Computed results were processed for statistical analysis using the Statistics MATLAB Toolbox. As statistical inference procedures, both one- and two-way ANOVA (estimate of within-group and between-group variance, on the basis of one dependent measure) and MANOVA (estimate of variance in multiple dependent parameters across groups) were used to assess the statistical significance of differences between groups. The corresponding statistical significance test [i.e., the $F_{[(m-1),(m-1)\times(n-1),(I-m)]}$ statistics and the resulting probability $P < p$ at the predetermined significance level $p < 0.05$] was performed, with sessions as repeated measures, coupled with contrast analysis when appropriate (Grafen and Hails 2002; Hair et al. 1998). The orders m (number of groups), n (number of mice), and I (number of multivariate observations) were reported accompanying the F-statistic values (Sánchez-Campusano et al. 2007). Wilk's lambda criterion and its transformation to the χ^2 distribution used in MATLAB were used to extract significant differences from MANOVA results (cluster analysis for cells–classes–spikes classification) during the spike-sorting problem in the phase space.

Multivariate analyses of electrophysiological signals

Multivariate analysis is extensively used with the aim of studying the relationship between simultaneously recorded signals or their equivalent time series. Multivariate time series tools (*nonlinear association analysis*) enabled us to determine the functional relatedness, asymmetry, time delay, and direction in coupling between neuronal multiunitary activities generated in red and interpositus nuclei and conditioned eyelid responses recorded across classical conditioning sessions. In practice, we have illustrated the use of multivariate analyses for assessing the strength (strong, moderate, or weak), type (linear or nonlinear), and direction in coupling (unidirectional or bidirectional) between these physiological time series.

We used nonlinear correlation analysis to investigate the following dynamic associations.

1 $Y_{OO\ EMG}(t)$ versus $X_{RN\ MUA}(t)$: between the EMG activity of the OO muscle and the neuronal MUA of red nucleus (RN).

2 $Y_{OO\ EMG}(t)$ versus $X_{IP\ MUA}(t)$: between the EMG activity of the OO muscle and the neuronal MUA of interpositus nucleus (IP).

3 $Y_{RN\ MUA}(t)$ versus $X_{IP\ MUA}(t)$: between the neuronal MUA of red nucleus (RN) and the neuronal MUA of interpositus nucleus (IP).

The nonlinear association index ($\eta^2_{\langle Y|X\rangle}$) between the electrophysiological signals $X(t)$ and $Y(t)$ was computed as

$$\eta^2_{\langle Y|X\rangle} = 1 - \frac{\sum_{j=1}^{Nb}\sum_{k\in B_j}[Y_k - \Im(X_j)]^2}{\sum_{k=1}^{Ns}(Y_k - \bar{Y})^2} \qquad (1)$$

where Ns is the number of samples of the signals, $\bar{Y}$ is the average of all amplitudes Y_k, and $\Im(X_j)$ is the piecewise approximation of the nonlinear regression curve. In *Eq. 1*, Nb is the number of bins and B_j (with $j = 1, \ldots, Nb$) represents the different bins in the corresponding scatter representations (for details, see Supplemental APPENDIX S2). The measure of association in the opposite direction $\eta^2_{\langle X|Y\rangle}$ can be calculated analogously. In this formulation, the subindex $\langle Y|X\rangle$ denotes the coupling from signal $X(t)$ to the signal $Y(t)$, $\langle X|Y\rangle$ indicates the coupling in the opposite direction—that is, from signal $Y(t)$ to the signal $X(t)$—and $\langle\_|\_\rangle$ denotes any one of the two directions of coupling.

To assess the direction of coupling between the electrophysiological signals $X(t)$ and $Y(t)$, we used the following direction index (Wendling et al. 2001)

$$D = \frac{1}{2}[\mathrm{sgn}(\Delta\eta^2) + \mathrm{sgn}(\Delta\tau)] \qquad (2)$$

where $\Delta\eta^2 = \eta^2_{\langle Y|X\rangle} - \eta^2_{\langle X|Y\rangle}$ and $\Delta\tau = \tau_{\langle Y|X\rangle} - \tau_{\langle X|Y\rangle}$, where $\tau_{\langle Y|X\rangle}$ (corresponding to $\eta_{\langle Y|X\rangle}$ and $\eta^2_{\langle Y|X\rangle}$) and $\tau_{\langle X|Y\rangle}$ (corresponding to $\eta_{\langle X|Y\rangle}$ and $\eta^2_{\langle X|Y\rangle}$) represent the time delays (i.e., the time shift $\tau_{\langle\_|\_\rangle}$ for which $\eta^2_{\langle\_|\_\rangle}(\tau)$ is maximum) between signals.

Indeed, if $X(t)$ causes $Y(t)$, $\tau_{\langle Y|X\rangle}$ will be positive and $\tau_{\langle X|Y\rangle}$ will be negative, so that the difference $\Delta\tau$ will also be positive. In this case, the degree of asymmetry of the nonlinear coupling $\Delta\eta^2$ will also be positive and therefore the direction index $D = +1$. These five previous conditions ($\tau_{\langle Y|X\rangle} > 0$; $\tau_{\langle X|Y\rangle} < 0$; $\Delta\tau > 0$; $\Delta\eta^2 > 0$; and $D = +1$) should be satisfied simultaneously, to conclude that the relationship is of the type $X(t) \rightarrow$YES $Y(t)$, i.e., a unidirectional coupling between signals (see Supplemental Fig. S3*A*). In all the other combinations of conditions, the relationship will be false [i.e., a spurious unidirectional coupling, $X(t) \rightarrow Y(t)$; see Supplemental Fig. S3, *B* and *C*].

If $Y(t)$ causes $X(t)$, $\tau_{\langle Y|X\rangle}$ will be negative and $\tau_{\langle X|Y\rangle}$ will be positive, so that the difference $\Delta\tau$ will also be negative. In this case, the degree of asymmetry of the nonlinear coupling $\Delta\eta^2$ will also be negative and, as a consequence, $D = -1$. These five previous conditions ($\tau_{\langle Y|X\rangle} < 0$; $\tau_{\langle X|Y\rangle} > 0$; $\Delta\tau < 0$; $\Delta\eta^2 < 0$; and $D = -1$) should be satisfied simultaneously, to conclude that the relationship is of the type $Y(t) \rightarrow$YES $X(t)$, that is, a unidirectional coupling between

signals (see Supplemental Fig. S3*D*). In all the other combinations of conditions, the relationship will be false [i.e., a spurious unidirectional coupling, $Y(t) \rightarrow\rightarrow X(t)$; see Supplemental Fig. S3, *E* and *F*].

If a feedback relationship between the signals $X(t)$ and $Y(t)$ is verified, then the time delays $\tau_{\langle Y|X\rangle}$ and $\tau_{\langle X|Y\rangle}$ will be positive, so that $\text{sgn}(\Delta\tau) \neq \text{sgn}(\Delta\eta^2)$ and therefore the direction index $D = 0$. The five previous conditions [($\tau_{\langle Y|X\rangle} > 0$; $\tau_{\langle X|Y\rangle} > 0$; $\Delta\tau < 0$; $\Delta\eta^2 > 0$; and $D = 0$) or ($\tau_{\langle Y|X\rangle} > 0$; $\tau_{\langle X|Y\rangle} > 0$; $\Delta\tau > 0$; $\Delta\eta^2 < 0$; and $D = 0$)] should be satisfied simultaneously, to conclude that the relationship is of the type $X(t) \rightarrow$YES $Y(t)$, i.e., a bidirectional coupling or a feedback relationship between signals. If the signal $Y(t)$ can be explained by the preceding signal $X(t)$ better than vice versa, then $X(t) \rightarrow$YES $Y(t)$ (see Supplemental Fig. S3*G*) and in the contrary case $X(t) \rightarrow$YES $Y(t)$ (see Supplemental Fig. S3*J*). In all the other combinations of conditions, the relationship will be false [i.e., a spurious bidirectional coupling, $X(t) \rightarrow(?)\ Y(t)$; see Supplemental Fig. S3, *H–I* and *K–L*].

The statistical significance tests (i.e., Student's *t*-test and *F*-statistic) were performed for the parameters of nonlinear correlation analysis. The hypothesis test was done by using the modified Fisher's w-transformation ($w_{\langle\_|\_\rangle}$) to associate each measured nonlinear association index ($\eta_{\langle\_|\_\rangle}$) with a corresponding $w_{\langle\_|\_\rangle}$ function

$$W_{\langle\_|\_\rangle} = \frac{1}{2}\ln\left(\frac{\eta_{\langle\_|\_\rangle}}{1-\eta_{\langle\_|\_\rangle}}\right) \quad \text{with } \eta\text{-linear dependence} \qquad (3)$$

$$W_{\langle\_|\_\rangle} = \frac{1}{2}\ln\left(\frac{\eta^2_{\langle\_|\_\rangle}}{1-\eta^2_{\langle\_|\_\rangle}}\right) \quad \text{with } \eta\text{-square dependence} \qquad (4)$$

Then, the functions $w_{\langle\_|\_\rangle}$ were approximately normally distributed with values within [−inf +inf]. The significance level (*P*) at which a measured value of $\eta_{\langle\_|\_\rangle}$ differs from some hypothesized value $\eta^{true}_{\langle\_|\_\rangle}$ (i.e., the actual or population value of the association index) was calculated using the complementary error functions for $w_{\langle\_|\_\rangle}$ and their mean value. Similarly, the significance of a difference between two measured nonlinear association indices ($\eta_{\langle Y|X\rangle}$ and $\eta_{\langle X|Y\rangle}$) was calculated using the corresponding functions $w_{\langle Y|X\rangle}$ and $w_{\langle X|Y\rangle}$ and the complementary error functions for pairs of means of samples (see Supplemental APPENDIX S2 for details).

If the probability *P* was less than the predetermined significance level (0.05), then the null hypothesis 1 (*H*0, that is, no difference between the measured $\eta_{\langle\_|\_\rangle}$ and the actual $\eta^{true}_{\langle\_|\_\rangle}$ values of the association index) and the null hypothesis 2 (*H*0, that is, no difference between two measured nonlinear association indices, $\eta_{\langle Y|X\rangle}$ and $\eta_{\langle X|Y\rangle}$) were rejected (Belsley et al. 1980). Small values of *P* indicate a significant difference. In all cases, if $H0 = 0$, we did not reject the null hypothesis. If $H0 = 1$, we rejected the null hypothesis.

One-way ANOVA *F*-tests were used to assess the statistical significance of differences among $w_{\langle\_|\_\rangle}$ functions with a null hypothesis 3 (*H*0, that is, no difference between populations means). In addition, the true statistical information about which particular pairs of means are significantly different and which are not (according to $\eta_{\langle\_|\_\rangle}$ and their $w_{\langle\_|\_\rangle}$ functions) was obtained with "multiple-comparison" analysis (see Supplemental APPENDIX S2).

Mean and SE values for $\eta_{\langle\_|\_\rangle}$ and $\tau_{\langle\_|\_\rangle}$ were calculated for all the trials presenting conditioned responses and collected from the same conditioning session for all the animals (i.e., three pairs of mean correlation curves and therefore six mean values of $\eta_{\langle\_|\_\rangle}$ and six mean values of $\tau_{\langle\_|\_\rangle}$ for each session). For all analyses, the amplitude of the signals $X(t)$ and $Y(t)$ was subdivided into 10 bins and the corresponding piecewise approximation (LPA for linear and nLPA for nonlinear piecewise approximations) of the nonlinear regression curve (Sánchez-Campusano et al. 2009) was calculated. Here we approximate the nonlinear dependence with segments of straight lines and/or with third-degree polynomials. For estimation of $\eta_{\langle\_|\_\rangle}$ we found out the best nonlinear fit assuming that $Y(t)$ is approximated with a third-degree polynomial of $X(t)$. The order of the nonlinear polynomial was selected after checking that for third-order approximation all the estimated coefficients remained statistically different from zero at the predetermined significance level of 0.05.

The nonlinear index $\eta_{\langle\_|\_\rangle}$ ranges from 0 (when the two signals are independent) to 1 (for a perfect dependence between the signals). A threshold value for the nonlinear index was set as criterion of significant association ($\eta_{\max\langle\_|\_\rangle} \geq 0.45$) and, progressively, the following distribution of the values: $0.45 \leq \eta_{\max\langle\_|\_\rangle} < 0.6$, that is, the two electrophysiological signals were slightly dependent (weak correlation) with low values of the maximum association index; $0.6 \leq \eta_{\max\langle\_|\_\rangle} < 0.75$, that is, the signals were moderately dependent (moderate correlation) with intermediate values of the maximum association index; and $0.75 \leq \eta_{\max\langle\_|\_\rangle} < 1.0$, that is, the signals were considerably dependent (strong correlation) with high values of the maximum association index. If the association index values were high in a direction and middle in the opposite direction, then we say that the signals were reasonably related (strong–moderate correlation). In the same way, if the index values were middle in a direction and low in the opposite direction, then we say that the signals were discretely related (moderate–weak correlation).

To determine whether time delays differed significantly from 0, the 95% confidence interval for $\tau_{\langle\_|\_\rangle}$ was measured for each pair of electrophysiological recordings per trial. The index $\eta_{\langle\_|\_\rangle}$ was recalculated (as function of the time shift) for various relative offsets of $X(t)$ and $Y(t)$ signals in 1-ms steps (one redefined uniform time of sampling for all the signals) from −250 to +250 ms, that is, the dynamic correlation range. The zero reference point within the correlation range indicates the onset of the conditioned response (see arrow in Fig. 3 and Supplemental APPENDIX S1).

RESULTS

Comparison of reflexively evoked eyelid responses in wild-type and Lurcher mice after the lesion of the interpositus nucleus

We tested the functionality of neural circuits involved in reflex eyelid responses in both wild-type and Lurcher animals following the lesion of the interpositus nucleus. Electrical stimulation of the supraorbital nerve in wild-type control mice (i.e., wild-type mice with no lesion in the interpositus nucleus) evoked an early OO EMG activation at a latency of 6.21 ± 0.19 ms (R1 component; see Kugelberg 1952), followed by a second EMG activation (R2 component), with a latency from the stimulus of 14.55 ± 0.01 ms (Fig. 4).

A two-way ANOVA *F*-test [$H0 = 1$, $F_{(3,69,1229)} = 22.19$, $P < 0.05$] indicated that Lurcher control mice (i.e., Lurcher mice with no lesion in interpositus nucleus) presented latencies for the R1 component (6.28 ± 0.11 ms) of the blink reflex that were similar to those of controls. However, and in accordance with a previous report (Porras-Garcia et al. 2005), those for the R2 component were significantly longer (16.43 ± 0.01 ms; $P < 0.05$). The mean amplitude of the R1 response in wild-type controls (0.82 ± 0.07 mV) was similar to that evoked in Lurcher control mice (0.86 ± 0.05 mV), whereas R2 responses in wild-type animals (1.10 ± 0.06 mV) were significantly larger than those for Lurcher control mice (0.65 ± 0.04 mV; $P < 0.05$). It has already been suggested that these performance deficits in the R2 component of reflexively evoked blinks could be related to a functional deficit in the projection to the reticular formation from cerebellar structures involved in the corneal reflex and, by extension, in the startle response (Porras-García et al. 2005).

The lesion of the interpositus nucleus had no significant effects on the latency of the R1 component for wild-type (lesioned

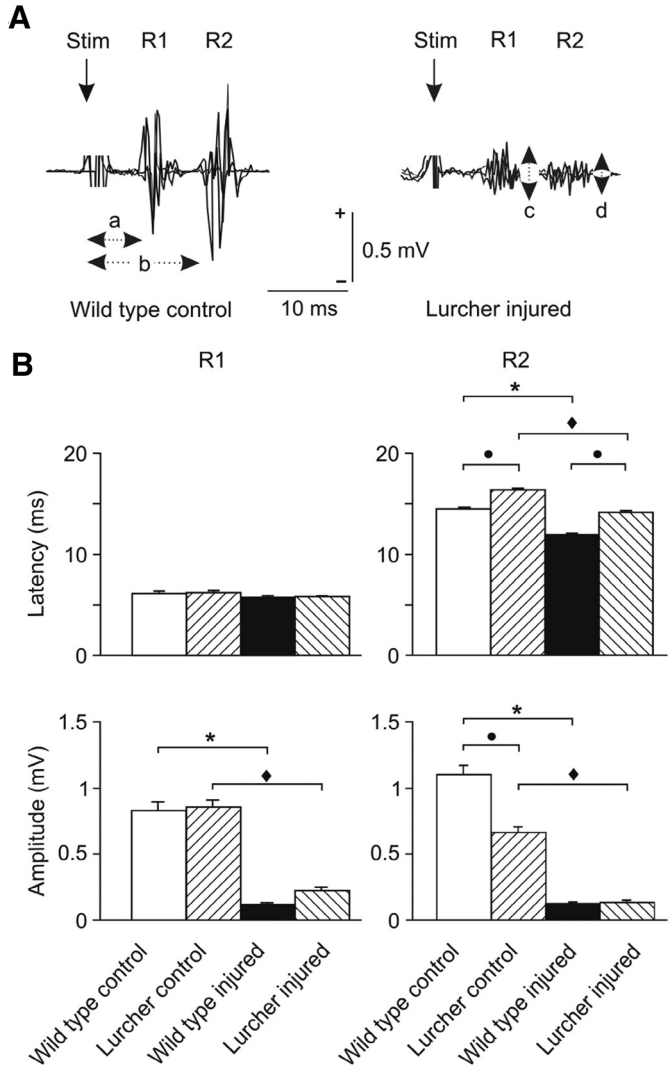

FIG. 4. Reflexively evoked blinks in wild-type and Lurcher mice with an interpositus nucleus lesion or without it (controls). *A*: 3 superimposed EMG traces recorded from the OO muscle of a nonlesioned wild-type animal (*left*) and of a Lurcher animal with an interpositus nucleus lesion (*right*) following electrical stimulation (a single, 500-μs cathodic pulse, 2 $\times$ threshold) of the supraorbital nerve. Note the characteristic R1 and R2 components. The latencies of R1 (*a*) and R2 (*b*) components, as well as their respective amplitudes (*c* and *d*), were quantified. *B*: mean values collected for latency and amplitude of both R1 and R2 components from electrically evoked blinks in the 4 groups of mice. A 2-way ANOVA *F*-test [$H0 = 1$, $F_{(3,69,1229)} = 22.19$, $P < 0.05$] indicates the following significant differences: $\rightarrow$, between Lurcher and wild-type mice (i.e., in the absence of any interpositus nucleus lesion); *, between lesioned wild-type animals and their nonlesioned controls; and ♦ between lesioned Lurcher animals and their controls (i.e., nonlesioned Lurcher mice).

wild-type = 5.83 ± 0.09 ms) or Lurcher mice (lesioned Lurcher = 5.90 ± 0.13 ms). The significant differences in the latency of the second component of the blink reflex between wild-type and Lurcher mice were maintained ($P < 0.05$) after the lesion of the interpositus nucleus (lesioned wild-type = 11.94 ± 0.14 ms; lesioned Lurcher = 14.11 ± 0.26 ms).

The lesion of the interpositus nucleus caused a significant ($P < 0.05$) decrease in the amplitude of the R1 component in lesioned wild-type (0.11 ± 0.01 mV) and in Lurcher mice (0.22 ± 0.01 mV), but also in the amplitude of R2 (lesioned wild-type = 0.13 ± 0.01 mV; lesioned Lurcher = 0.14 ± 0.01 mV; $P <$ 0.05). Accordingly, having blink circuits with apparently normal functional properties, Lurcher mice exhibited less efficiency in the execution of the late (R2) component of the reflex eyelid responses with and without the interpositus nucleus. Moreover, the appearance of the blink reflex responses after electrical stimulation of the supraorbital nerve suggests that the interpositus nucleus is not necessary for the generation of blink motor responses, but the lack of this nucleus changes the kinematics (latency and amplitude) of those reflex responses.

Lesion of the interpositus nucleus prevents the classical conditioning of eyelid responses

We compared the learning capabilities of wild-type and Lurcher mice with those of animals lacking the interpositus nucleus, using a delayed conditioning paradigm (Fig. 1*C*). Control and sham groups of wild-type (Fig. 5*A*) and Lurcher (Fig. 5*B*) mice presented a significant increase in the percentage of conditioned responses from the fourth session on for wild-type and from the sixth session on for Lurcher mice [two-way ANOVA *F*-test, $H0 = 1$, $F_{(13,299,826)} = 1,84$, $P <$ 0.05]. It should be noted that the insertion of stimulating electrodes in the interpositus nucleus in sham animals did not disturb their learning capabilities. As a whole, wild-type and Lurcher mice presented learning curves similar to those described previously in this species (Chen et al. 1996; Domínguez-del-Toro et al. 2004; Kishimoto et al. 2002; Porras-Garcia et al. 2005; Takatsuki et al. 2003). However, in coincidence with a previous report (Porras-García et al. 2005), the increase in the percentage of conditioned responses in the Lurcher mice (control and sham) was more gradual, reaching asymptotic values from the sixth session on. Although asymptotic values reached in Lurcher mice were lower than those reached by controls, no significant differences between their respective learning curves were noticed. In this regard, it has been proposed recently (Sakamoto and Endo 2008) that the decrease of γ-aminobutyric acid (GABA) receptors could be related with their slightly lower rate in the generation of CRs.

In contrast, lesioned wild-type (Fig. 5*A*) and Lurcher (Fig. 5*B*) mice were unable to acquire conditioned responses across training, presenting no significantly different values from those collected during habituation sessions. As illustrated in Fig. 1*A*, those lesions were centered in the posterior subdivision of the interpositus nucleus, although in 20% of the cases the lesion also reached the anterior part of the nucleus as well as the most medial part of the deep cerebellar lateral nucleus.

Both red and interpositus nuclei are involved in the acquisition and execution of conditioned eyelid responses in wild-type and Lurcher mice

To determine the participation of red and interpositus nuclei neurons in eyelid conditioning, we recorded the MUA in both nuclei during the acquisition of this type of associative learning. The final location of those recording electrodes is illustrated in Fig. 6*A* and Supplemental Fig. S2, *A–D*. In accordance with a recent retrograde transneuronal tracing study (Morcuende et al. 2002), electrodes recording neuronal firing related to eyelid movements were located preferentially at the dorsolateral aspect of the red nucleus and in the posterior subdivision of the interpositus nucleus, as well as in the caudal aspects of its anterior subdivision.

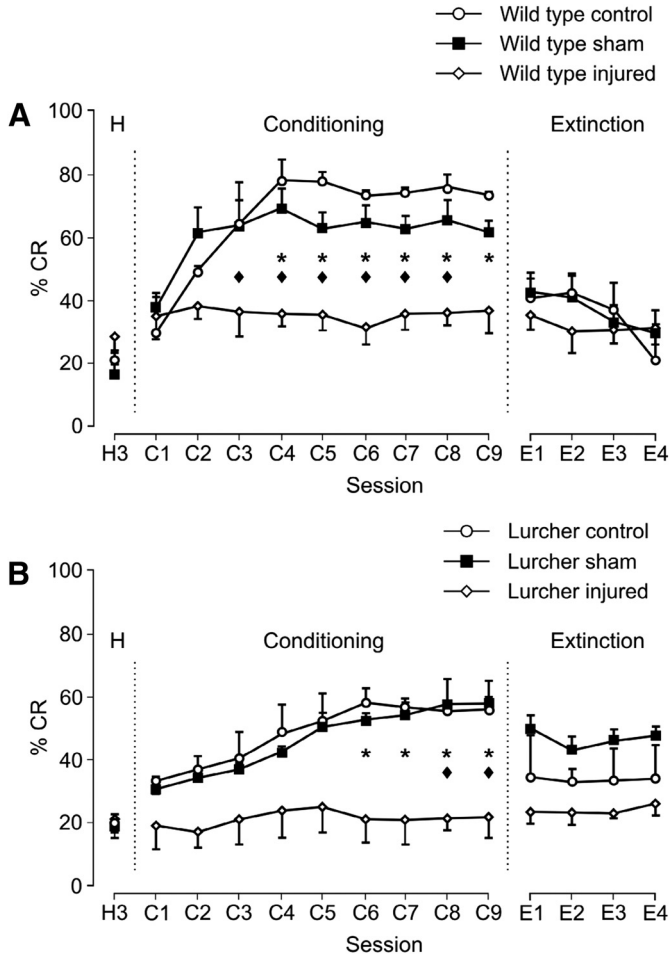

FIG. 5. Learning curves for lesioned and nonlesioned wild-type and Lurcher mice. The evolution of the percentage of conditioned responses (% CRs ± SE) across the successive sessions for wild-type (*A*) and Lurcher (*B*) mice is shown. H3 represents data from the 3rd habituation session, C1–C9 represent conditioning sessions, and E1–E4 represent data from extinction sessions. A 2-way ANOVA *F*-test [$H0 = 1$, $F_{(13,299,826)} = 1.84$, $P < 0.05$] indicates that there were no significant differences between control and sham groups for both wild-type and Lurcher mice, but there were significant differences between control and sham with respect to lesioned mice. *, significant differences between control and lesioned animals (for wild-type and Lurcher mice); and ♦, significant differences between sham and lesioned animals (also for wild-type and Lurcher mice).

As illustrated in Fig. 7*C*, both wild-type and Lurcher mice presented learning curves similar to those shown previously by control and sham-lesioned wild-type (Fig. 5*A*) and Lurcher (Fig. 5*B*) animals. Although the two groups of animals presented a similar mean percentage of conditioned responses (CRs: 21.67 ± 1.67% for wild-type and 24.33 ± 2.39% for Lurcher) during the habituation session, they reached asymptotic values at different times (by the third session for wild-type and by the fifth for Lurcher mice). Nevertheless, there were no significant differences between the two groups, except for the third session (Fig. 7*C*). Percentages of CRs recorded in the ninth session were statistically different from those in the third session for wild-type and from the fourth for Lurcher mice [two-way ANOVA *F*-test, $H0 = 1$, $F_{(9,45,890)} = 2.06$, $P < 0.05$].

Furthermore, for the neuronal MUAs (e.g., Fig. 7, *A* and *B*) we analyzed the results of the spike-pattern classification method (see an application of the spike-sorting algorithm in Fig. 8 and METHODS for details). The time–frequency spectrograms and spike-sorting tools allowed us to identify the spike patterns of activity of red and interpositus neurons, including the number of neurons per animal and the spike events for each single neuron across the conditioning process. The mean num-

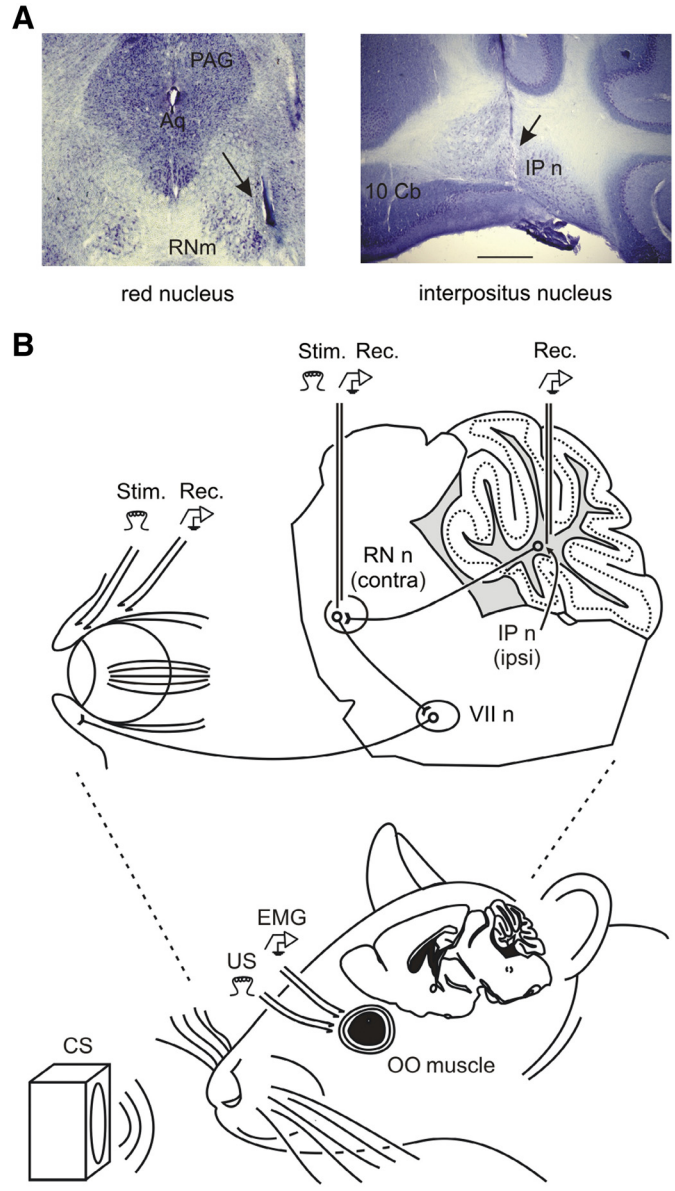

FIG. 6. Experimental model for recording the firing activities of interpositus (IP n) and red (RN n) nuclei neurons during classical conditioning of eyelid responses in wild-type and Lurcher mice. *A*: photomicrographs of Nissl staining illustrating the location of the recording electrodes (arrows) in the red nucleus (*left*) and in the interpositus nucleus (*right*) in a wild-type mouse. Calibration bar = 500 μm. *B*: diagrammatic representation of the experimental design. Bipolar electrodes were aimed at both nuclei (IP n and RN n) with the help of stereotaxic coordinates and stimulating and recording procedures. Animals were also implanted with EMG recording electrodes in the OO muscle and with stimulating electrodes on the ipsilateral supraorbital nerve. The latter was used for US presentation. For classical conditioning of eyelid responses, we used a tone (250 ms; 2.4 kHz; 85 dB) as CS and an electric shock (500 μs, 3 × threshold) as US. Aq, aqueduct of Sylvius; PAG, periaqueductal gray; RNm, red nucleus magnocellular part; VII n, facial nucleus; 10Cb, 10th cerebellar lobule; Stim., stimulating sites; Rec., recording sites.

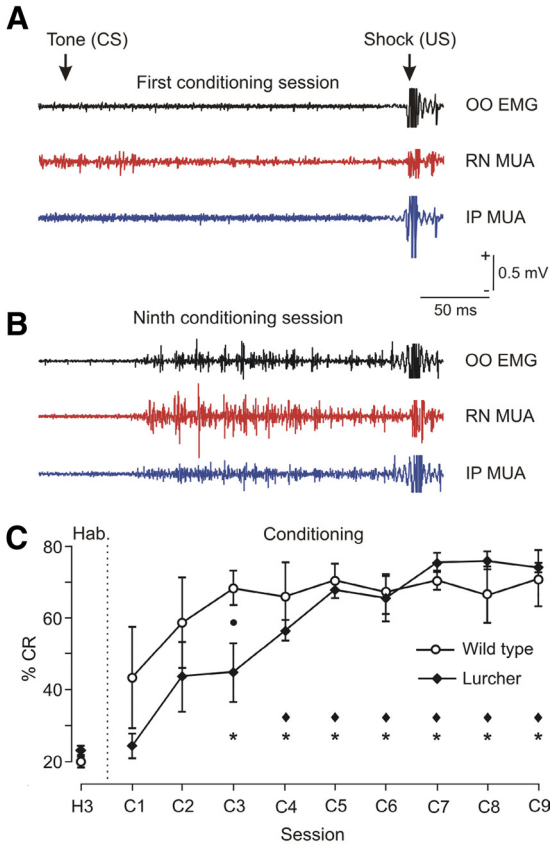

FIG. 7. Firing activities in red and interpositus nuclei during the acquisition of conditioned eyelid responses in both wild-type and Lurcher mice. *A*: an example of delay conditioning with indication of CS (tone, 250 ms, 2.4 kHz, 85 dB) and US (electric shock, 500 μs, 3 $\times$ threshold) presentations. Traces illustrate the EMG activity of the OO muscle (OO EMG, black trace) and the multiunitary activity (MUA) recorded in the red (RN MUA, red trace) and in the interpositus (IP MUA, blue trace) nuclei. Records were collected during the 1st conditioning session from a representative wild-type mouse. Note the absence of any conditioned activity. *B*: the same as in *A*, but from the 9th conditioning session. In this case, the presence of OO EMG and MUA in RN and IP is evident. *C*: evolution of percentage of conditioned responses (% CR $\pm$ SE) across training for both wild-type and Lurcher mice. H3 represents data from the 3rd habituation session, whereas C1–C9 represents conditioning sessions. Differences between wild-type and Lurcher mice ($\rightarrow$) were not statistically different, except for the 3rd conditioning session [2-way ANOVA *F*-test, $H0 = 1$, $F_{(9,45,890)} = 2.06$, $P < 0.05$]. * Significant differences in the percentage of CRs (% CR) between conditioning sessions and the H3 session for wild-type mice and ♦, the same for Lurcher mice.

bers of neurons detected per session and related to eyelid responses were 2.1 (i.e., 17 neurons related to eyelid responses collected from the eight animals across training) for red nucleus and 2.7 (i.e., 22 neurons) for interpositus nucleus, but with a bimodal distribution of their spikes in the CS–US interval. Also, the relative refractory periods of neurons (i.e., minimum interspike interval) were in the ranges 6.0–8.4 ms (for interpositus neurons) and 4.9–5.7 ms (for red nucleus neurons). As described in detail in the following text, the onset of modulation of neuronal activity and their peak frequency showed that both red and interpositus nuclei during performance of the conditioned response always lagged the beginning and peak amplitude of the evoked eyelid responses.

A representation of the different parameters collected across conditioning sessions is depicted in Fig. 9*A*, for both wild-type

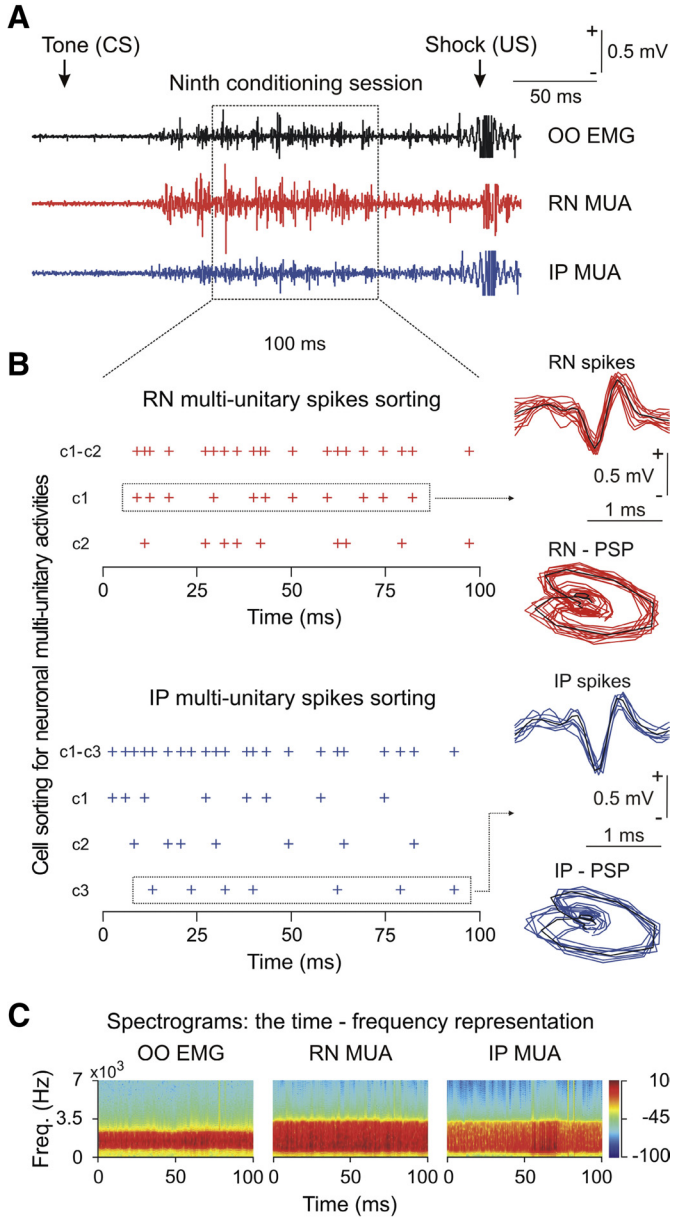

FIG. 8. *A*: the traces illustrate the electromyographic activity of the orbicularis oculi muscle (OO EMG, black trace) and the recordings of the red nucleus multiunitary activity (RN MUA, red trace) and the identified cerebellar interpositus nucleus multiunitary activity (IP MUA, blue trace) collected from the 9th conditioning session of a representative wild-type mouse. A random window of 100 ms of duration is marked (dotted rectangle) over the recordings containing the spikes in the CS–US interval. This representative temporal window was used to show the spike-pattern classification method. *B*: application of a spike-sorting algorithm that identifies the spike patterns of activity in the 2 nuclei of neurons determines the number of neurons and assigns each spike event to a particular neuron. The action-potential pulses marked with red "+" signs correspond to the direct representation of the neural activity in the red nucleus (2-cell sorting: c1–c2) and the action potential pulses recorded from the interpositus nucleus (3-cell sorting: c1–c3) are indicated with blue "+" signs. The 2 dotted horizontal rectangles indicate the selection of all of the spikes (11 RN and 7 IP spikes, red and blue curves, respectively) and the average spike (black curve) waveforms for a single neuron (c1, for RN MUA; c3, for IP MUA) from each one of the multiunitary activities. In addition, the phase space portraits (PSPs) for the RN and IP spike waveforms are represented. *C*: the time–frequency spectrograms for the 3 electrophysiological signals (sample frequencies at 14 kHz) are illustrated, with a predominant frequency band of 500–3,500 Hz (i.e., spike waveforms of duration $\leq$2.0 ms) for the whole dynamic range.

and Lurcher mice. For example, for wild-type data the mean peak firing rate of interpositus neurons [parameter 1, one-way ANOVA F-test, $H0 = 1$, $F_{(8,16,576)} = 13.21$, $P < 0.01$] increased across conditioning. In contrast, the mean number of spikes (parameter 2) generated by interpositus neurons in CS–US interval changed significantly [$H0 = 1$, $F_{(8,16,576)} = 2.37$, $P < 0.05$] across conditioning but without a clear tendency, suggesting that the increase in their firing rate after CS presentation represented a reorganizing (instead of a net increase) of their mean spontaneous firing. Finally, an inverted evolution was obtained for the latency of the maximum instantaneous frequency for the interpositus neurons in the CS–US interval [parameter 3; $H0 = 1$, $F_{(8,16,576)} = 3.93$, $P < 0.01$]. Interestingly, the total number of spikes generated by red nucleus neurons (parameter 5) during the CS–US interval increases across conditioning sessions [$H0 = 1$, $F_{(8,16,576)} = 2.11$, $P < 0.05$] and their mean peak firing rate (parameter 4) also increases [$H0 = 1$, $F_{(8,16,576)} = 9.27$, $P < 0.01$], indicating that this premotor red nucleus was implicated as a candidate drives (kinetic neural command) the eyelid conditioned response. However, the latency of the maximum instantaneous frequency (parameter 6) for red nucleus neurons in the CS–US interval remained invariable across training [one-way ANOVA F-test, $H0 = 0$, $F_{(8,16,576)} = 1.17$, $P < 0.05$].

As illustrated in the bottom part of Fig. 9*A*, Lurcher mice presented a similar evolution across conditioning with respect to the same parameters indicated earlier, with the following statistical values: 1, $H0 = 1$, $F_{(8,16,576)} = 7.94$, $P < 0.05$; 2, $H0 = 1$, $F_{(8,16,576)} = 2.48$, $P < 0.05$; 3, $H0 = 1$, $F_{(8,16,576)} = 12.29$, $P < 0.01$; 4, $H0 = 1$, $F_{(8,16,576)} = 5.15$, $P < 0.01$; 5, $H0 = 1$, $F_{(8,16,576)} = 2.36$, $P < 0.05$; and 6, $H0 = 0$, $F_{(8,16,576)} = 1.06$, $P > 0.05$.

The evolution of these parameters (1, 3, 4, and 5) across conditioning was analogous to that observed previously, using the same classical conditioning paradigm (Domínguez-del-Toro et al. 2004; Gruart et al. 1995; Sánchez-Campusano et al. 2009). Note that in Fig. 9*A*, the parameters were normalized according to their maximum values. For example, in wild-type data, the maximum values of mean peak of the firing rate were 166.6 spikes/s (parameter 1, session C8) and 205.1 spikes/s (parameter 4, session C7) for both interpositus and red nucleus neurons, respectively. In Lurcher data, the values of the mean peak of firing rate (parameters 1 and 4) decreased in the two nuclei of neurons (interpositus neurons, 119.2 spikes/s, session C9; red nucleus neurons, 175.3 spikes/s, session C8) with respect to the values of these parameters in wild-type data. In both wild-type and Lurcher mice, the maximum values of the mean latencies of the maximum instantaneous frequencies (parameter 6) for the interpositus neurons were 226.5

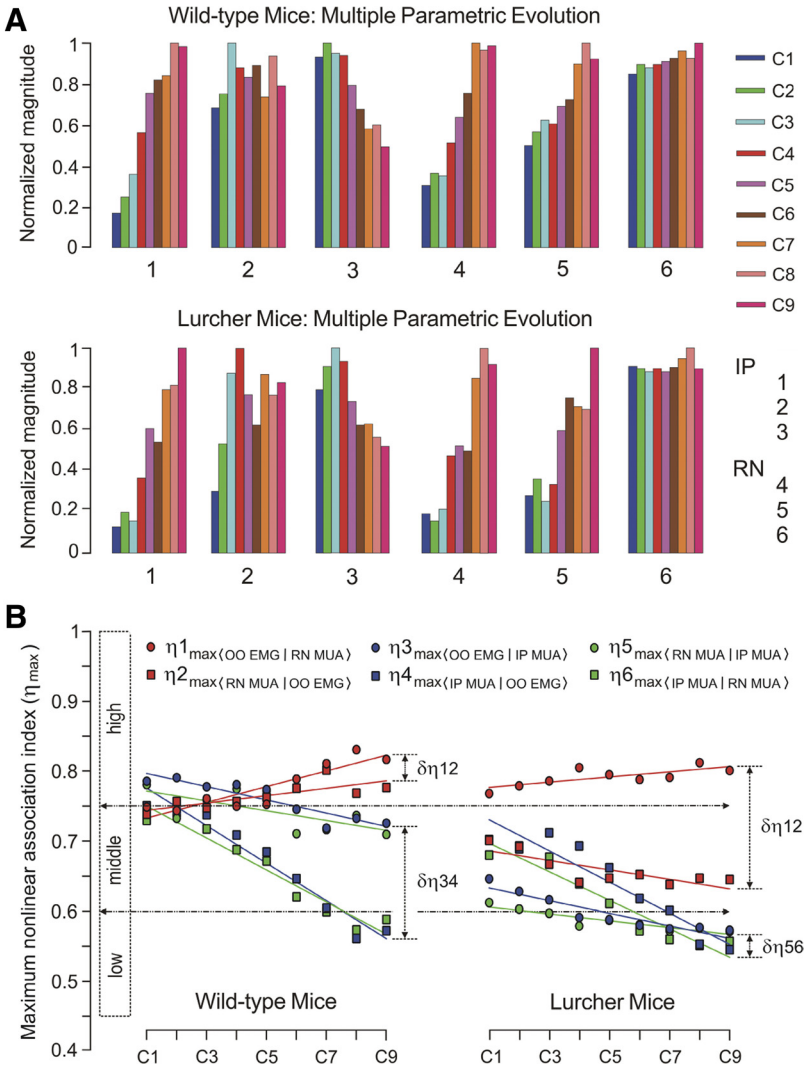

FIG. 9. A representation of multiparametric evolution of results collected across conditioning sessions. *A*: the color code indicates the corresponding conditioning session (C1–C9); each set of color bars corresponds to the evolution of a given parameter (numbered from 1 to 6); and each color bar indicates the mean parametric value resulting from averaging the trials of the same session, a procedure applied for each of the sessions. The parameters 1 and 4 (mean peak firing rate, in spikes/s), 2 and 5 (total number of spikes in the CS–US interval), and 3 and 6 (latency of the maximum value of mean firing rate with respect to CS presentation, in ms) were calculated for both interpositus (IP) and red nucleus (RN) neurons. For this representation, the parameters have been normalized according to their maximum absolute values in the corresponding set and for the 2 data model (wild-type and Lurcher mice). *B*: the maximum values of nonlinear association indices (η_{max}) and their variations across training. The 3 ranges of maximum index values (high, middle, and low) are indicated. The color code indicates the 3 dynamic associations (red, for RN MUA vs. OO EMG; blue, for IP MUA vs. OO EMG; green, for IP MUA vs. RN MUA). Each color circle corresponds to the maximum value of association index in the preferential direction of coupling and each color square indicates the maximum values of association index in the opposite direction. The color lines represent the linear regression models (tendency analysis) for each set of maximum association indices across conditioning sessions. The magnitudes $\delta\eta12$, $\delta\eta34$, and $\delta\eta56$ indicate the difference between the pairs of maximum association indices at the asymptotic level of acquisition of this associative learning test (session C9) in both wild-type and Lurcher data.

ms (in session C2) and 231.1 ms (in session C3). The maximum values of mean number of spikes generated by red nucleus neurons in the CS–US interval (parameter 5) were 19.1 spikes (in session C8) for wild-type data and 21.3 spikes (in session C9) for Lurcher data.

Measuring directional coupling among simultaneously recorded electrophysiological signals during the classical conditioning of eyelid responses

In the previous sections, we have presented results related to the level of expression of eyelid conditioned responses in the different experimental groups (wild-type vs. Lurcher and lesioned vs. nonlesioned; see Figs. 5, *A* and *B* and 7*C*) and the acquisition and representation of the physiological multiparametric data collected across conditioning sessions (Figs. 7–9). These results (the learning curves and the quantitative multiparametric analyses) were necessary but insufficient for a precise functional discrimination between the two groups of animals (wild-type and Lurcher mice, Fig. 7*C*) and for an appropriate dynamic description of the conditioning process. In this section, we use an analytical approach (the nonlinear multivariate analysis of electrophysiological recordings) to understand the functional correlation code and the directional coupling mechanisms between the EMG activity of the OO muscle and crude recordings of MUAs in both red and interpositus nuclei and between the two neuronal MUA recordings during the classical conditioning of eyelid responses in wild-type and Lurcher mice.

The degree of association between the EMG activity of the OO muscle [$Y_{OO\ EMG}(t)$] and crude recordings of neuronal responses [$X_{MUA}(t)$] collected from red [$X_{RN\ MUA}(t)$] and interpositus [$X_{IP\ MUA}(t)$] nuclei neurons was obtained by computing the nonlinear association index ($\eta_{\langle \_|\_ \rangle}$) as a function of a time shift ($\tau_{\langle \_|\_ \rangle}$) between these muscular and multiunitary neuronal signals. Also, the association between the two neuronal MUAs was analyzed [$Y_{RN\ MUA}(t)$ vs. $X_{IP\ MUA}(t)$ and vice versa]. The shift for which the maximum of $\eta_{\langle \_|\_ \rangle}(\tau)$ was reached provided an estimate of the time delay between these electrophysiological signals during the associative learning process in wild-type and Lurcher mice. Thus we were able to determine whether the maximum nonlinear correlation between MUAs in red and interpositus nuclei and EMG activities was before or after the zero reference point (i.e., the moment at which the conditioned eyelid response started; see arrow in Fig. 3). To check whether the EMG recordings of OO muscle carried out here were representative of actual eyelid responses, we recorded in some animals ($n = 3$) eyelid responses with the magnetic search-coil technique (see Gruart et al. 1995 for details and references) simultaneously with EMG records. Collected eyelid responses were similar in profiles and latencies with those recorded from mice using the magnetic distance measurement technique (see Boele et al. 2010 for details).

As illustrated in Fig. 3*F* and in Supplemental Fig. S2, eyelid movements recorded with the magnetic search-coil technique followed the EMG activity of the OO muscle with a latency of 5.9 ms. For technical reasons, since the magnetic search-coil technique could not be used during MUA recordings, all analyses related to the initiation of the CR were carried out with data collected from OO EMG recordings.

The nonlinear association functions corresponding to the trials taken from the same session were averaged, session by session and for each experimental subject. The present study was centered on the analysis of data collected at CS–US intervals (Fig. 7, *A* and *B*) across the nine sessions (C1–C9). In Fig. 9*B*, we represent the maximum values of nonlinear association indices (η_{max}) and their evolution across training. The maximum indices between MUA of red nucleus neurons and OO EMG remained with high values across conditioning sessions in both wild-type and Lurcher mice. However, the increase in the mean peak firing rate of interpositus neurons (parameter 1 in Fig. 9*A*) together with the decrease in its time of occurrence (parameter 3 in Fig. 9*A*, always lagged the start of CR) caused a decrease in the nonlinear association indices between MUA of interpositus neurons and eyelid conditioned responses (determined by OO EMG activity) in both wild-type and Lurcher mice (Fig. 9*B*). A standard analysis of the tendencies using linear regression models allowed us to determine the evolution of the η_{max} across training. For example, the blue and green lines (between the interpositus MUA and either OO EMG or red nucleus MUA, respectively) showed clear negative slopes and therefore a decrease of correlation levels according with nonlinear correlation analysis. In addition, the red lines (MUA of red nucleus neurons vs. OO EMG) showed a moderate tendency to increase in wild-type data, but their tendencies were opposed for Lurcher data (see the parameters of this tendency analysis, i.e., the correlation coefficients, the significances, and the equations of the regression lines, in Supplemental Table S1). Furthermore, in this study we also developed in detail the specific nonlinear association analysis for the data at the asymptotic level of acquisition (i.e., the ninth conditioning session) of this associative learning test.

In Figs. 10*A* and 11*A* are represented the nonlinear correlation analysis carried out with OO EMG records (corresponding to conditioned responses) and crude recordings of multiunitary neuronal activity (in both red and interpositus nuclei) collected during the ninth conditioning session in both wild-type and Lurcher mice. As illustrated in Figs. 10*A* and 11*A*, the nonlinear association curves ranged from 250 ms before to 250 ms after the zero reference point. This representation enabled us to determine the time of occurrence of the maximum nonlinear correlation ($\eta_{max\langle \_|\_ \rangle}$ index)—i.e., the time of delay in coupling between EMG and multiunitary neuronal signals and also between the neuronal MUAs in both red and interpositus nuclei. The first and second of the illustrated curves (red traces, in both Fig. 10*A* and Fig. 11*A*) correspond to the nonlinear association curves between OO EMG [$Y_{OO\ EMG}(t)$] and red nucleus MUA [$X_{RN\ MUA}(t)$]. The third and fourth curves (blue traces, in both Fig. 10*A* and Fig. 11*A*) represent the nonlinear association curves between OO EMG [$Y_{OO\ EMG}(t)$] and interpositus MUA [$X_{IP\ MUA}(t)$], whereas the other two (fifth and sixth curves, green traces, in Figs. 10*A* and 11*A*) correspond to the nonlinear association curves between red nucleus MUA [$X_{RN\ MUA}(t)$] and interpositus MUA [$X_{IP\ MUA}(t)$].

For the nonlinear association curves shown in Figs. 10*A* and 11*A*, the null hypothesis was rejected for all the functions $w_{\langle \_|\_ \rangle}$ of the nonlinear association indices $\eta_{\langle \_|\_ \rangle}$ obtained during the ninth conditioning session in wild-type and Lurcher mice [modified Fisher's *z*-tests, $H0 = 1$, $P_m\{[w1], [w2], [w3], [w4], [w5], [w6]\} < 0.05$, with m = wt (for wild-type mice) or m = Lc (for Lurcher mice); see Figs. 10*B*, 11*B*, and 12, *A* and *B* and Supplemental APPENDIX S2].

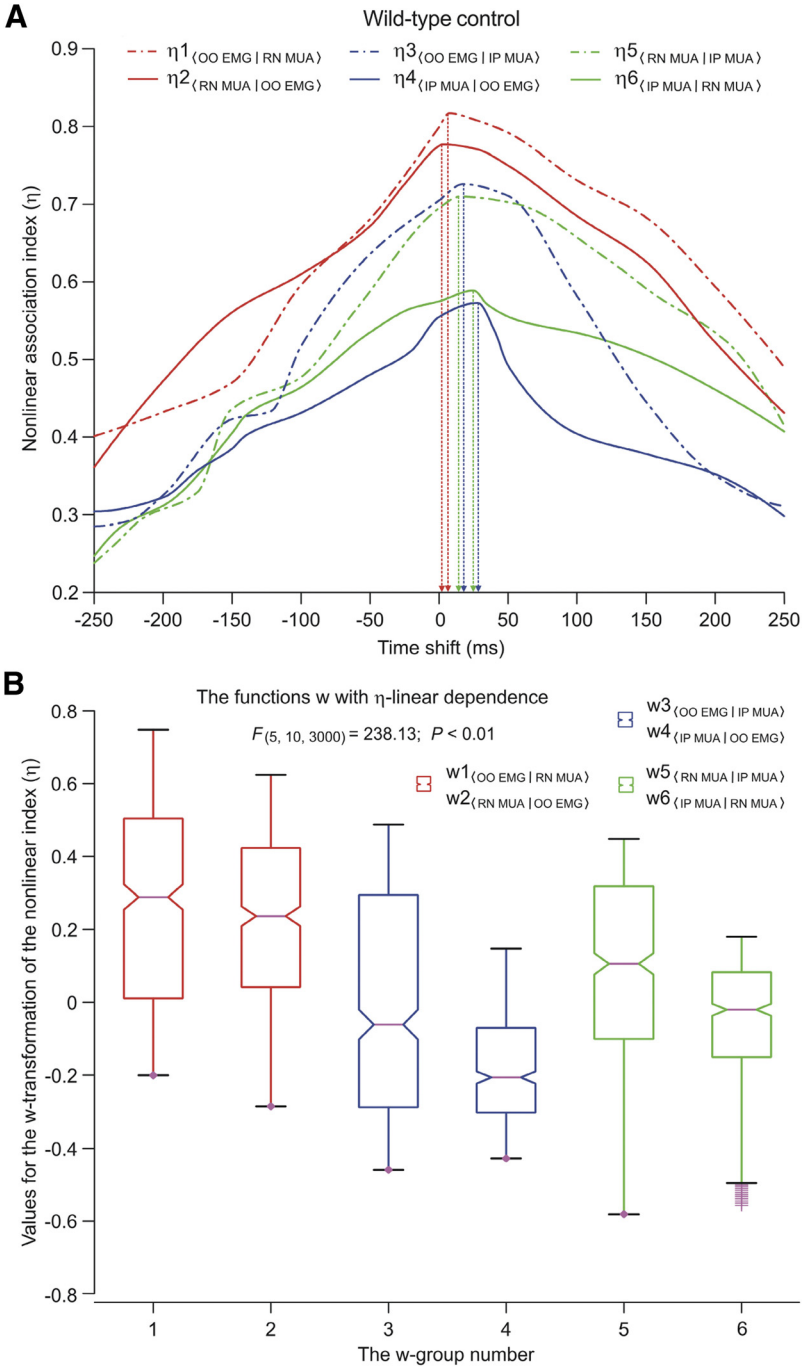

FIG. 10. A representation of the nonlinear association method applied to the EMG activity of the OO muscle (OO EMG) and MUA recorded from red nucleus (RN MUA) or interpositus (IP MUA) neurons for the wild-type data. *A*: the nonlinear association indices (η) were calculated for the 3 pairs of electrophysiological signals (in both directions) as functions of the time shift. The start of the conditioned response (determined by the EMG activity of the OO muscle) is taken as the zero reference point of the dynamic association. Six nonlinear association curves are represented. Each representation corresponds to the average of all nonlinear association curves obtained for the trials presenting conditioned responses and collected from the same conditioning session for all the animals (wild-type, 3 mice, C9). The vertical broken lines represent the time shifts for which the maximum values for nonlinear association indices are reached (time delays). In the first case (red curves, OO EMG vs. RN MUA and vice versa), the information of asymmetry and the relative time delay in coupling were positive [$\Delta(\eta 12)^2 > 0$, $\Delta\tau 12 > 0$, respectively], whereas the index of directional coupling between the signals was equal to unity ($D_{12} = +1$). In the second case (blue curves, OO EMG vs. IP MUA and vice versa), the degree of asymmetry of the nonlinear coupling was positive [$\Delta(\eta 34)^2 > 0$] and the relative time delay between the signals was negative ($\Delta\tau 34 < 0$), so that the direction index was annulled ($D_{34} = 0$). In the third case (green curves, RN MUA vs. IP MUA and vice versa), a bidirectional coupling was also clearly verified [$\Delta(\eta 56)^2 > 0$, $\Delta\tau 56 < 0$, and $D_{56} = 0$]. In all cases, the time delays are located to the right of the zero reference point (i.e., in both nuclei the activity always lagged the start of the conditioned response). *B*: the ANOVA test and the box plot [one-way ANOVA *F*-test, $H0 = 1$, $F_{(5,10,3000)} = 238.13$, $P < 0.01$] for the functions w (η-linear dependence) of the nonlinear association curves (in *A*). The box has lines at the lower quartile, median, and upper quartile values. The whiskers extending from each end of the box show the extent of the rest of the data. In this case, the estimated values of the medians were 0.2887 for w1, 0.2365 for w2, −0.0614 for w3, −0.2064 for w4, 0.1056 for w5, and −0.0207 for w6.

Furthermore, we found significant differences between the nonlinear association indices for the two possible directions of coupling in each signal pair—i.e., the determination of the probability P_m between $w_{\langle Y|X\rangle}$ versus $w_{\langle X|Y\rangle}$ (representing the transformations of $\eta_{\langle Y|X\rangle}$ and $\eta_{\langle X|Y\rangle}$, respectively) in both wild-type and Lurcher mice [paired modified Fisher's *z*-tests, $H0 = 1$, $P_m\{[w1, w2], [w3, w4], [w5, w6]\} < 0.05$, for $\eta 1_{\langle OO\ EMG|RN\ MUA\rangle}$ vs. $\eta 2_{\langle RN\ MUA|OO\ EMG\rangle}$; $\eta 3_{\langle OO\ EMG|IP\ MUA\rangle}$ vs. $\eta 4_{\langle IP\ MUA|OO\ EMG\rangle}$; $\eta 5_{\langle RN\ MUA|IP\ MUA\rangle}$ vs. $\eta 6_{\langle IP\ MUA|RN\ MUA\rangle}$]. However, when analyzing exclusively the mean values of nonlinear association indices across the dynamic range, we demonstrated by "multiple-comparisons" analysis (see Supplemental APPENDIX S2) that there was no significant difference between groups w1 and w2 for the wild-type mice [refer to Table 1 (for ≤99% confidence interval and η-linear dependence), Fig. 12*A*, Supplemental Table S2 (for ≤95% confidence interval and η-square dependence), and Supplemental Fig. S4*A*]. For the Lurcher mice, the difference between w3 and w5 groups was also not significant according to the results indicated in Table 2 (for a 99% confidence interval and η-linear dependence), Fig. 12*B*, Supplemental Table S3 (for a 95% confidence interval and η-square dependence), and Supplemental Fig. S4*B*. The results of standard ANOVA tests are summarized in Supplemental Table S4.

These results enabled us to determine how the changes in the correlation code level (loss or gain of asymmetry) during the

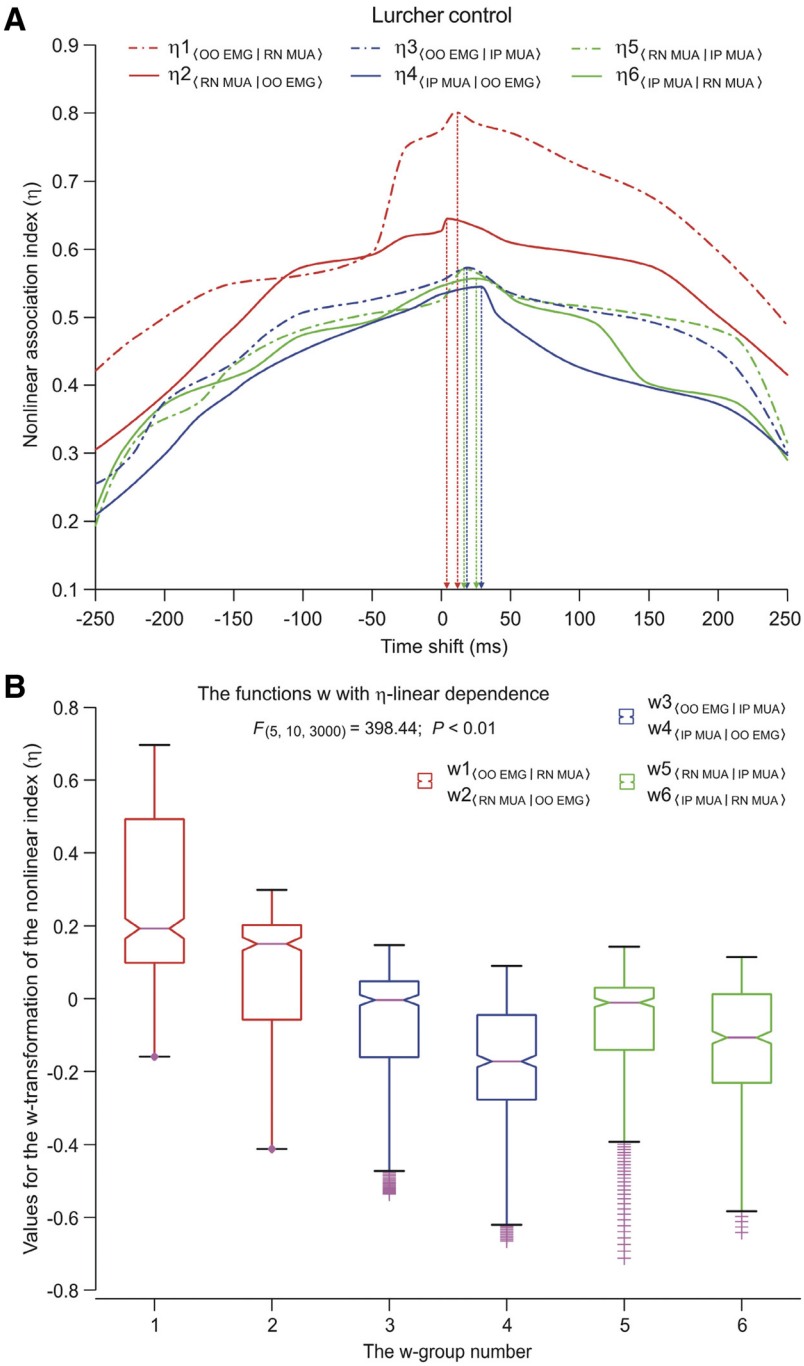

FIG. 11. A representation of the nonlinear association method applied to the EMG activity of the OO muscle (OO EMG) and to the MUA recorded from red nucleus (RN MUA) or interpositus (IP MUA) neurons for the Lurcher data. *A*: the nonlinear association indices (η) were calculated for the 3 pairs of electrophysiological signals (in both directions) as functions of the time shift. The start of the conditioned response (OO EMG) is taken as the zero reference point of the dynamic association. Six nonlinear association curves are represented. Each representation corresponds to the average of all nonlinear association curves obtained for the trials presenting conditioned responses and collected from the same conditioning session for all the animals (Lurcher, 3 mice, C9). The vertical broken lines represent the time delays. In the first case (red curves, OO EMG vs. RN MUA and vice versa), the information of asymmetry and the relative time delay in coupling were positive and very significant [22.6%, $\Delta(\eta 12)^2 > 0$, $\Delta\tau 12 > 0$, respectively], whereas the index of the directional coupling between the signals was equal to unity ($D_{12} = +1$). In the second case (blue curves, OO EMG vs. IP MUA and vice versa), the degree of asymmetry of the nonlinear coupling was positive but very poor [3.1%, $\Delta(\eta 34)^2 > 0$] and the relative time delay between the signals was negative ($\Delta\tau 34 < 0$), so that the direction index was annulled ($D_{34} = 0$). In the third case (green curves, RN MUA vs. IP MUA and vice versa), a bidirectional coupling was also clearly verified [very poor asymmetry information (1.6%), $\Delta(\eta 56)^2 > 0$, $\Delta\tau 56 < 0$, and $D_{56} = 0$]. In all cases, the time delays are located to the right of the zero reference point (i.e., in both nuclei the activity always lagged the beginning of the conditioned response). *B*: the ANOVA test and the box plot [one-way ANOVA *F*-test, $H0 = 1$, $F_{(5,10,3000)} = 398.44$, $P < 0.01$] for the functions w (η-linear dependence) of the nonlinear association curves (in *A*). In this case, the estimated values of the medians were 0.1926 for w1, 0.1504 for w2, −0.0038 for w3, −0.1720 for w4, −0.0109 for w5, and −0.1066 for w6.

couplings between the MUA recorded in both red and interpositus nuclei and the learned motor response (OO EMG activity) and between the two neuronal MUAs could be induced by the cerebellar cortical degeneration present in Lurcher mice. For example, in Table 3 we summarize the qualitative results of the nonlinear correlation analysis including the strength, the type, and the direction in coupling for all the dynamic associations in both wild-type and Lurcher mice during the ninth conditioning session.

Dynamic associations among neuronal MUAs and EMG responses in wild-type mice

Dynamic association functions enabled us to describe how the mean nonlinear association indices ($\eta_{\langle\_|\_\rangle}$) evolved during the successive sessions (see Fig. 9*B*). Three general nonlinear correlation analyses were made for wild-type animals. In the first analysis (OO EMG vs. red nucleus MUA and vice versa), the correlation functions evolved from middle ($0.6 < \eta_{\max\langle\_|\_\rangle} < 0.75$, C1–C3) to high ($0.75 < \eta_{\max\langle\_|\_\rangle} < 1$, C4–C9) values of maximum association indices across conditioning sessions; i.e., the two electrophysiological signals were considerably dependent (strong correlation) and their coupling was relatively symmetric at the asymptotic level of acquisition of this associative learning test (session C9). Moreover, red nucleus MUAs correlated significantly [one-way ANOVA *F*-tests, $H0 = 1$, $F_{(8,16,576)} = 7.21$, $P < 0.01$, for $\eta_{\max\langle\text{OO EMG}|\text{RN MUA}\rangle}$; and $H0 = 1$, $F_{(8,16,576)} = 2.41$, $P < 0.05$, for $\eta_{\max\langle\text{RN MUA}|\text{OO EMG}\rangle}$] with the OO EMG activity

TABLE 1. *Characteristic values of the multiple-comparisons algorithm (η-linear dependence) for the functions w1–w6 of the nonlinear association indices during the ninth conditioning session for wild-type data*

Wild-Type (Fig. 10*B*)		99% Confidence Interval for the Difference in Means		
w-Groups (η-Linear Dependence)		Smallest Value	Estimated Difference in Means	Largest Value
w1	w2	−0.0141	0.0396	0.0933
w1	w3	0.2205	0.2742	0.3279
w1	w4	0.3993	0.4530	0.5067
w1	w5	0.1516	0.2053	0.2590
w1	w6	0.2818	0.3355	0.3892
w2	w3	0.1809	0.2346	0.2883
w2	w4	0.3598	0.4135	0.4672
w2	w5	0.1121	0.1658	0.2195
w2	w6	0.2422	0.2959	0.3496
w3	w4	0.1251	0.1788	0.2325
w3	w5	−0.1226	−0.0689	−0.0152
w3	w6	0.0075	0.0612	0.1149
w4	w5	−0.3014	−0.2477	−0.1940
w4	w6	−0.1713	−0.1176	−0.0639
w5	w6	0.0764	0.1301	0.1838

Functions w1–w6 refer to the w-groups shown in Fig. 10*B*. The nonlinear association indices η1–η6 are shown in Fig. 10*A*.

during the performance of conditioned responses in all the conditioning sessions. Notably, their time delays in the two directions of coupling were always positive and therefore a spurious unidirectional coupling from signal $X_{RN\ MUA}(t)$ to signal $Y_{OO\ EMG}(t)$ was verified. In this relationship, we confirmed that a strong correlation is necessary but insufficient to reveal the direction of coupling and the true causal inference between signals. In the second analysis (OO EMG vs. interpositus MUAs and vice versa), the maximum values of the nonlinear association indices were statistically significant [one-way ANOVA *F*-tests, $H0 = 1$, $F_{(8,16,576)} = 17.86$, $P < 0.01$, for $\eta_{max\langle OO\ EMG|IP\ MUA\rangle}$; and $H0 = 1$, $F_{(8,16,576)} = 21.09$, $P < 0.01$, for $\eta_{max\langle IP\ MUA|OO\ EMG\rangle}$], although their values showed a clear transition from a strong correlation ($0.75 < \eta_{max\langle OO\ EMG|IP\ MUA\rangle} < 1$, C1–C5) to a moderate correlation ($0.6 < \eta_{max\langle OO\ EMG|IP\ MUA\rangle} < 0.75$, C6–C9) in the preferential direction of coupling. In the opposite direction, the maximum index values determined an evolution from a moderate correlation ($0.6 < \eta_{max\langle IP\ MUA|OO\ EMG\rangle} < 0.75$, C1–C7) to a weak correlation ($0.45 < \eta_{max\langle IP\ MUA|OO\ EMG\rangle} < 0.6$, C8–C9); i.e., two signals [$X_{IP\ MUA}(t)$ and $Y_{OO\ EMG}(t)$] were discretely related (a mixture between moderate and slight dependences during the ninth conditioning session) and their coupling was asymmetric. In this analysis, the maximum association index values always lagged the zero reference point across the successive conditioning sessions. In the third analysis (red nucleus vs, interpositus MUAs and vice versa), the maximum association indices also evolved from high ($\eta_{max\langle RN\ MUA|IP\ MUA\rangle} > 0.75$) to intermediate ($0.6 < \eta_{max\langle RN\ MUA|IP\ MUA\rangle} < 0.75$) values in the preferential direction of coupling and from intermediate ($0.6 < \eta_{max\langle IP\ MUA|RN\ MUA\rangle} < 0.75$) to low ($0.45 < \eta_{max\langle IP\ MUA|RN\ MUA\rangle} < 0.6$) values in the opposite direction; i.e., the two electrophysiological signals were also discretely related and their coupling was also asymmetric during the ninth conditioning session. In addition, the differences among the mean values of the maximum nonlinear association indices were statistically significant [one-way ANOVA *F*-tests, $H0 = 1$, $F_{(8,16,576)} = 2.28$, $P < 0.05$, for $\eta_{max\langle RN\ MUA|IP\ MUA\rangle}$; and $H0 = 1$, $F_{(8,16,576)} = 20.05$, $P < 0.01$, for $\eta_{max\langle IP\ MUA|RN\ MUA\rangle}$] across conditioning sessions and their corresponding time delays

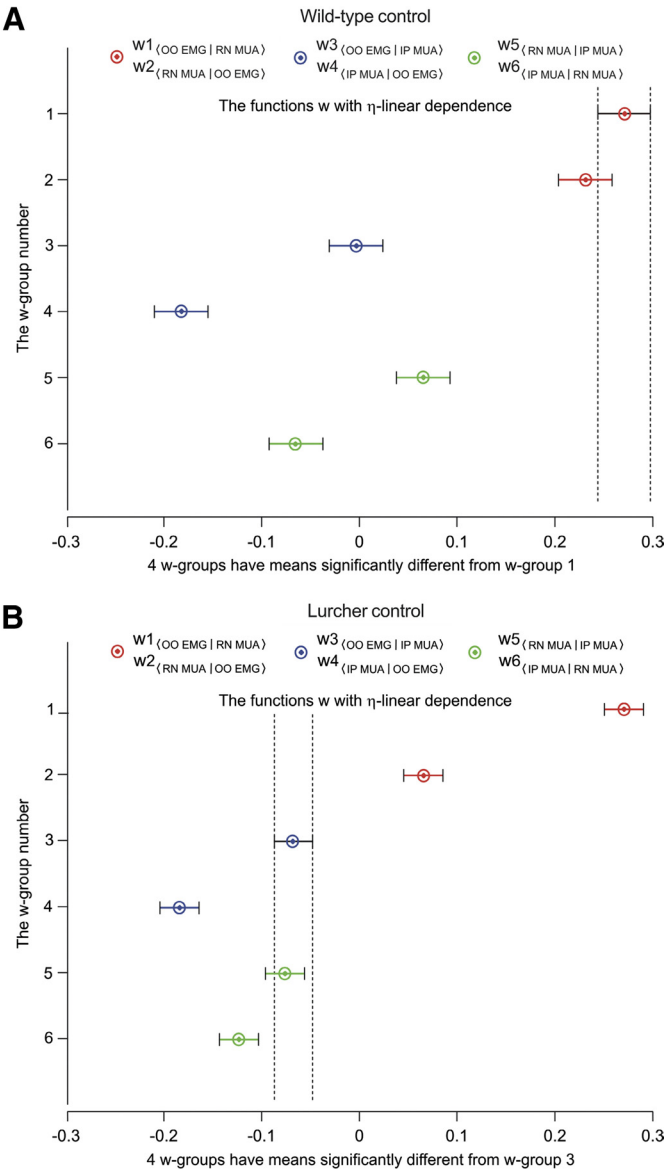

FIG. 12. The multiple comparison procedure for the nonlinear association curves of Figs. 10*B* (wild-type) and 11*B* (Lurcher) and their functions w (see *Eq. 3* with η-linear dependence). The multiple-comparison graph and the quantitative analysis (rows of the output matrix in Table 1 for wild-type data and in Table 2 for Lurcher data) show that 14 of the comparisons involving the 6 groups (w1–w6) have confidence intervals that do not include zero, so the difference is significant at the 0.01 level (a 99% confidence interval for the estimated true difference in means). In other words, we can reject the null hypothesis that the true difference is zero and therefore those differences are significant, with the exceptions of the comparison between the w1 and w2 groups for wild-type data (in *A*) and of the comparison between the w3 and w5 groups for Lurcher data (in *B*). *A*: for the wild-type data, the estimated values of the means were 0.2707 for w1, 0.2312 for w2, −0.0035 for w3, −0.1823 for w4, 0.0654 for w5, −0.0647 for w6, and the SE was 0.0113 (see the confidence intervals for the difference in means in Table 1). *B*: for the Lurcher data, the estimated values of the means were 0.2717 for w1, 0.0663 for w2, −0.0667 for w3, −0.1835 for w4, −0.0755 for w5, −0.1227 for w6, and the SE was 0.0082 (see the confidence intervals for the difference in means in Table 2). Two means are significantly different if their intervals are disjoint and are not significantly different if their intervals overlap.

TABLE 2. *Characteristic values of the multiple-comparisons algorithm (η-linear dependence) for the functions w1–w6 of the nonlinear association indices during the ninth conditioning session for Lurcher data*

Lurcher (Fig. 11*B*) w-Groups (η-Linear Dependence)		99% Confidence Interval for the Difference in Means		
		Smallest Value	Estimated Difference in Means	Largest Value
w1	w2	0.1662	0.2054	0.2445
w1	w3	0.2992	0.3384	0.3776
w1	w4	0.4160	0.4552	0.4943
w1	w5	0.3081	0.3472	0.3864
w1	w6	0.3552	0.3944	0.4336
w2	w3	0.0939	0.1331	0.1722
w2	w4	0.2106	0.2498	0.2890
w2	w5	0.1027	0.1419	0.1811
w2	w6	0.1499	0.1891	0.2282
w3	w4	0.0776	0.1167	0.1559
w3	w5	−0.0303	0.0088	0.0480
w3	w6	0.0168	0.0560	0.0952
w4	w5	−0.1471	−0.1079	−0.0687
w4	w6	−0.0999	−0.0608	−0.0216
w5	w6	0.0080	0.0472	0.0863

Functions w1–w6 refer to the w-groups shown in Fig. 11*B*. The nonlinear association indices η1–η6 are shown in Fig. 11*A*.

in the two directions of coupling always lagged the zero reference point. In the second and third analyses, the information of asymmetry and the time delays in coupling allowed us to verify the clear bidirectional coupling between the $X_{IP\ MUA}(t)$ and either $X_{RN\ MUA}(t)$ or $Y_{OO\ EMG}(t)$.

In the first dynamic association [$Y_{OO\ EMG}(t)$ vs. $X_{RN\ MUA}(t)$, red curves in Fig. 10*A*] at the asymptotic level of acquisition of this associative learning test, the maximum association indices remained with high values in the dynamic correlation range [paired modified Fisher's *z*-test, $H0 = 1$, $P_{wt}[w1, w2] < 0.05$, for the significance of a difference between two measured association indices; means ± SE, $\eta 1_{max\langle OO\ EMG|RN\ MUA\rangle} = 0.817 \pm 0.004$ and $\eta 2_{max\langle RN\ MUA|OO\ EMG\rangle} = 0.777 \pm 0.009$]. As a result, the information of asymmetry for the maximum values of the nonlinear association indices [$\Delta(\eta 12)^2 = \eta I^2_{max\langle OO\ EMG|RN\ MUA\rangle} - \eta 2^2_{max\langle RN\ MUA|OO\ EMG\rangle} \approx 0.064$; i.e., the OO EMG response variations can be explained by the preceding red nucleus neuronal activity practically with the same strength that vice versa] showed a deviation of only 6.4% (i.e., one signal can be explained as a quasi-linear transformation of the other). The time delay in the direction of preferential coupling was positive [mean ± SE, $\tau 1_{\langle OO\ EMG|RN\ MUA\rangle} = 7.32 \pm 0.07$ ms; i.e., the signal $X_{RN\ MUA}(t)$ preceding the signal $Y_{OO\ EMG}(t)$], but the time delay in the opposite direction was also positive [mean ± SE, $\tau 2_{\langle RN\ MUA|OO\ EMG\rangle} = 2.22 \pm 0.13$ ms; i.e., the signal $Y_{OO\ EMG}(t)$ also preceding the signal $X_{RN\ MUA}(t)$]. These data are clearly indicative of a spurious unidirectional coupling ($\Delta\tau 12 \approx 5.10$ ms and $D_{12} = +1$) between the two electrophysiological signals [$X_{RN\ MUA}(t) \rightarrow (?)\ Y_{OO\ EMG}(t)$] during the ninth conditioning session, a result that was verified across the preceding conditioning sessions (data not shown). In summary, red nucleus MUA encodes EMG activity of the OO muscle, but a strong correlation and a positive time delay value were also confirmed in the opposite direction. This indicates that $D_{12} = +1$ but with $\tau 2_{\langle RN\ MUA|OO\ EMG\rangle} > 0$ and, consequently, the necessary causal conditions were not satisfied for a true unidirectional coupling neither for a bidirectional relationship ($D_{12} \neq 0$) between these signals.

In the second association [$Y_{OO\ EMG}(t)$ vs. $X_{IP\ MUA}(t)$, blue curves in Fig. 10*A*], the maximum nonlinear association indices were only moderately [from signal $X_{IP\ MUA}(t)$ to signal $Y_{OO\ EMG}(t)$] and weakly (in the opposite direction) significant in the dynamic correlation range [paired modified Fisher's *z*-test, $H0 = 1$, $P_{wt}[w3, w4] < 0.05$, for the significance of a difference between two measured nonlinear association indices; mean ± SE, $\eta 3_{max\langle OO\ EMG|IP\ MUA\rangle} = 0.726 \pm 0.018$ and $\eta 4_{max\langle IP\ MUA|OO\ EMG\rangle} = 0.573 \pm 0.013$]. The statistical algorithm developed here indicates that the degree of asym-

TABLE 3. *Qualitative report of the results obtained with the nonlinear correlation analysis at the asymptotic level of acquisition of the associative learning test (session C9)*

Association		Strength	Value	Dependence	Type	Symmetry	Direction
A. Wild-type: Animal model without cerebellar cortical degeneration							
1	η1	Strong	High	Considerable	Quasi-linear	Quasi-symmetric	Spurious unidirectional coupling
	η2	Strong	High				
2	η3	Moderate	Intermediate	Discretionary	Nonlinear	Asymmetric	Bidirectional coupling
	η4	Weak	Low				
3	η5	Moderate	Intermediate	Discretionary	Nonlinear	Asymmetric	Bidirectional coupling
	η6	Weak	Low				
B. Lurcher: Animal model with cerebellar cortical degeneration							
1	η1	Strong	High	Reasonable	Nonlinear	Asymmetric	Spurious unidirectional coupling
	η2	Moderate	Intermediate				
2	η3	Weak	Low	Slight	Quasi-linear	Quasi-symmetric	Bidirectional coupling
	η4	Weak	Low				
3	η5	Weak	Low	Slight	Quasi-linear	Quasi-symmetric	Bidirectional coupling
	η6	Weak	Low				

Reported results indicate the strength of coupling (strong, moderate, or weak correlation), the range of maximum index values (high, intermediate, or low), the dependence between the recordings (considerably, reasonable, moderately, discretely, or slightly dependent, in this order), the type of relationship (quasi-linear or nonlinear), the information of asymmetry (quasi-symmetric or asymmetric), and the direction in coupling (unidirectional or bidirectional) for all the dynamic associations in both wild-type and Lurcher mice (see in Fig. 9*B* the differences δη12, δη34, and δη56 between the nonlinear and association indices).

metry in coupling for the maximum values of the nonlinear association indices [$\Delta(\eta 34)^2 = \eta 3^2_{max\langle OO\ EMG|IP\ MUA\rangle} - \eta 4^2_{max\langle IP\ MUA|OO\ EMG\rangle} \approx 0.999$] presented a deviation of 19.9% (i.e., one signal can be explained as a transformation—possibly nonlinear—of the other). In the same way, the time delays in the two possible directions of coupling were also positive [mean ± SE, $\tau 3_{\langle OO\ EMG|IP\ MUA\rangle} = 17.25 \pm 0.31$ ms and $\tau 4_{\langle IP\ MUA|OO\ EMG\rangle} = 28.14 \pm 0.16$ ms; i.e., the signal $X_{IP\ MUA}(t)$ preceding the signal $Y_{OO\ EMG}(t)$ and vice versa], whereas the relative time delay was negative ($\Delta\tau 34 \approx -10.9$ ms). According to this analysis, the functional interdependence between the recorded signals was nonlinear and bidirectional [$D_{34} = 0$, $X_{IP\ MUA}(t) \rightarrow$YES $Y_{OO\ EMG}(t)$; i.e., OO muscle response variations can be explained by the preceding interpositus neurons activity better than vice versa] during the ninth training session, a result that was also verified for the preceding conditioning sessions (data not shown). In contrast with the first association, the bidirectional coupling indicated a feedback relationship between OO EMG and interpositus neuronal signals [$Y_{OO\ EMG}(t)$ and $X_{IP\ MUA}(t)$] recorded during the classical conditioning of eyelid responses. These data suggest that, instead of one signal exclusively driving the other, each signal [$Y_{OO\ EMG}(t)$ and $X_{IP\ MUA}(t)$] influences the other. According to these results, the bidirectional coupling between OO EMG and interpositus neuronal recordings [$Y_{OO\ EMG}(t)$ and $X_{IP\ MUA}(t)$] could be explained if we assume that there is an indirect reinforcement effect of interpositus neurons on facial OO motoneurons (Sánchez-Campusano et al. 2009).

In the third association (green curves in Fig. 10*A*), the functional interdependence between the simultaneously recorded signals [$X_{IP\ MUA}(t)$ and $X_{RN\ MUA}(t)$] was also bidirectional [$D_{56} = 0$, $X_{IP\ MUA}(t) \rightarrow$YES $Y_{RN\ MUA}(t)$; i.e., changes in the response of red nucleus neurons can be explained by the preceding activity in interpositus neurons better than vice versa]. The maximum nonlinear association indices were moderately [from signal $X_{IP\ MUA}(t)$ to signal $X_{RN\ MUA}(t)$] and slightly (in the opposite direction) significant in the dynamic correlation range (paired modified Fisher's *z*-test, $H0 = 1$, $P_{wt}[w5, w6] < 0.05$, for the significance of a difference between two measured nonlinear association indices; mean ± SE, $\eta 5_{max\langle RN\ MUA|IP\ MUA\rangle} = 0.710 \pm 0.021$ and $\eta 6_{max\langle IP\ MUA|RU\ MUA\rangle} = 0.589 \pm 0.027$). The degree of asymmetry in coupling for the maximum values of the nonlinear correlation indices [$\Delta(\eta 56)^2 = \eta 5^2_{max\langle RN\ MUA|IP\ MUA\rangle} - \eta 6^2_{max\langle IP\ MUA|RN\ MUA\rangle} \approx 0.157$] presented a deviation (in the nonlinear sense) of 15.7%. Additionally, the time delays in the two possible directions of coupling were also positive [mean ± SE, $\tau 5_{\langle RN\ MUA|IP\ MUA\rangle} = 15.16 \pm 0.09$ ms and $\tau 6_{\langle IP\ MUA|RN\ MUA\rangle} = 25.05 \pm 0.17$ ms; i.e., the signal $X_{IP\ MUA}(t)$ preceding the signal $X_{RN\ MUA}(t)$ and vice versa], whereas the relative time delay was negative ($\Delta\tau 56 \approx -9.89$ ms).

Finally, and according to the present results, the functions w1 and w2 (OO EMG vs. red nucleus MUA coupling and vice versa) for wild-type data did not show significant differences at the asymptotic level of acquisition of the conditioned response. Therefore the signals $X_{RN\ MUA}(t)$ and $Y_{OO\ EMG}(t)$ were considerably dependent (see Fig. 12*A*) with high values of the correlation coefficients and their relationship was relatively symmetric (quasi-linear interdependence), but their positive time delays only determined a spurious unidirectional coupling (see Table 3 for a qualitative report for all the associations from animal model without cerebellar cortical degeneration). However, the functions w3 and w4 (OO EMG vs. interpositus MUA coupling and vice versa) and the functions w5 and w6 (red nucleus MUA vs. interpositus MUA coupling and vice versa) for wild-type data showed significant differences ; i.e., a clear asymmetric interdependence between the $X_{IP\ MUA}(t)$ and either $Y_{OO\ EMG}(t)$ or $X_{RN\ MUA}(t)$, with a evident bidirectional coupling (see, Table 3) determined by the positive signs of their time delays. Regarding these results, we can infer that the high symmetry (low asymmetry between $\eta 1$ and $\eta 2$ association functions without significant differences between w1 and w2 functions; see Tables 1 and 3) in the OO EMG and red nucleus MUA coupling compensates, by modulation of the correlation code, the low symmetry (high asymmetry between $\eta 3$ and $\eta 4$ association functions with significant differences between w3 and w4 functions; see Tables 1 and 3) in the OO EMG and interpositus MUA coupling. The latter probably caused the low symmetry (high asymmetry between $\eta 5$ and $\eta 6$ association functions with significant differences between w5 and w6 functions; see Tables 1 and 3) in the red nucleus MUA and interpositus MUA coupling for the wild-type data.

Dynamic associations among neuronal MUAs and EMG responses in Lurcher mice

Three general nonlinear correlation analyses were also developed for Lurcher mice. In the first analysis (OO EMG vs. red nucleus MUA and vice versa), the maximum association index values remained considerably high ($0.75 < \eta_{max\langle OO\ EMG|RN\ MUA\rangle} < 1.0$) in the preferential direction of coupling, but in the opposite direction, a clear loss of correlation degree ($0.6 < \eta_{max\langle RN\ MUA|OO\ EMG\rangle} < 0.75$) was observed across conditioning sessions; i.e., the two electrophysiological signals were only reasonably dependent but with evident asymmetry during all of the conditioning sessions (Fig. 9*B*). Thus red nucleus MUA correlate significantly [one-way ANOVA *F*-tests, $H0 = 1$, $F_{(8,16,576)} = 2.11$, $P < 0.05$, for $\eta_{max\langle OO\ EMG|RN\ MUA\rangle}$; and $H0 = 1$, $F_{(8,16,576)} = 27.43$, $P < 0.01$, for $\eta_{max\langle RN\ MUA|OO\ EMG\rangle}$] with the EMG activity of the OO muscle during the performance of conditioned responses but with nonlinear dependence. Moreover, the time delays in the two directions of coupling were always positive and presented few variations with respect to the time delays in the wild-type mice; i.e., a spurious unidirectional coupling from signal $X_{RN\ MUA}(t)$ to signal $Y_{OO\ EMG}(t)$ was also verified, with an evident gain of asymmetry degree. In the second analysis (OO EMG vs. interpositus MUA and vice versa), the differences among the mean values of maximum nonlinear association indices were statistically significant [one-way ANOVA *F*-tests, $H0 = 1$, $F_{(8,16,576)} = 31.19$, $P < 0.01$, for $\eta_{max\langle OO\ EMG|IP\ MUA\rangle}$; and $H0 = 1$, $F_{(8,16,576)} = 49.55$, $P < 0.01$, for $\eta_{max\langle IP\ MUA|OO\ EMG\rangle}$] across conditioning sessions, although their magnitudes showed a restricted association from moderate correlation ($0.6 < \eta_{max\langle \_|\_\rangle} < 0.75$) to weak correlation ($0.45 < \eta_{max\langle \_|\_\rangle} < 0.6$) in the two directions of coupling; i.e., the two signals were slightly related at the asymptotic level of acquisition of this associative learning test and their functional coupling was practically symmetric. Again in this analysis, the maximum association index values always lagged the zero reference point across the successive conditioning sessions. In the third analysis (red nucleus MUA vs. interpositus MUA and vice versa), the maximum associa-

tion indices showed a transition from intermediate mean values ($0.6 < \eta_{\max\langle \_|\_ \rangle} < 0.75$) to relatively low mean values ($0.45 < \eta_{\max\langle \_|\_ \rangle} < 0.6$) across conditioning sessions; i.e., the two electrophysiological signals were also slightly related and with a quasi-symmetric coupling (see Fig. 9*B*). Nevertheless, the differences among the mean values of the nonlinear association indices were statistically significant [one-way ANOVA *F*-tests, $H0 = 1$, $F_{(8,16,576)} = 12.23$, $P < 0.01$, for $\eta_{\max\langle \text{RN MUA}|\text{IP MUA}\rangle}$; and $H0 = 1$, $F_{(8,16,576)} = 10.18$, $P < 0.01$, for $\eta_{\max\langle \text{IP MUA}|\text{RN MUA}\rangle}$] across conditioning sessions and their time delays always lagged the zero reference point. In the second and third analyses, the information of asymmetry and the time delays in coupling allowed us to verify the clear bidirectional coupling between the $X_{\text{IP MUA}}(t)$ and either $X_{\text{RN MUA}}(t)$ or $Y_{\text{OO EMG}}(t)$, but with loss of the asymmetry degree.

In the first association [$Y_{\text{OO EMG}}(t)$ vs. $X_{\text{RN MUA}}(t)$, red curves in Fig. 11*A*] at the asymptotic level of acquisition of this associative learning test, the maximum association indices remained with high values in the preferential direction of coupling [from signal $X_{\text{RN MUA}}(t)$ to signal $Y_{\text{OO EMG}}(t)$] and intermediate values in the opposite direction [paired modified Fisher's *z*-test, $H0 = 1$, $P_{\text{Lc}}[\text{w1, w2}] < 0.05$, for the significance of a difference between two measured nonlinear correlation coefficients; mean ± SE, $\eta 1_{\max\langle \text{OO EMG}|\text{RN MUA}\rangle} = 0.801 \pm 0.007$ and $\eta 2_{\max\langle \text{RN MUA}|\text{OO EMG}\rangle} = 0.645 \pm 0.022$]. Thus the statistical algorithm developed here indicates that the degree of asymmetry in coupling for the maximum values of the nonlinear correlation coefficients $[\Delta(\eta 12)^2 = \eta 1^2_{max\langle OO\ EMG|RN\ MUA\rangle} - \eta 2^2_{max\langle RN\ MUA|OO\ EMG\rangle} \approx 0.226$; i.e., OO EMG activity variations can be explained by the red nucleus MUA better than vice versa] presented a deviation of 22.6% (i.e., one signal can be explained as a transformation—possibly nonlinear—of the other). The time delay in the direction of preferential coupling was positive [mean ± SE, $\tau 1_{\langle \text{OO EMG}|\text{RN MUA}\rangle} = 10.20 \pm 0.11$ ms; i.e., the signal $X_{\text{RN MUA}}(t)$ preceding the signal $Y_{\text{OO EMG}}(t)$], but the time delay in the opposite direction was also positive [mean ± SE, $\tau 2_{\langle \text{RN MUA}|\text{OO EMG}\rangle} = 4.12 \pm 0.34$ ms, i.e., the signal $Y_{\text{OO EMG}}(t)$ also preceding the signal $X_{\text{RN MUA}}(t)$]. These data are clearly indicative of a spurious unidirectional coupling ($\Delta\tau 12 \approx 6.08$ ms and $D_{12} = +1$) between the two electrophysiological signals [$X_{\text{RN MUA}}(t) \rightarrow (?)\ Y_{\text{OO EMG}}(t)$] during the ninth conditioning session, a result that was verified across the preceding conditioning sessions (data not shown). In summary, red nucleus MUA encodes EMG activity of the OO muscle, but the positive sign of the time delay in the opposite direction ($t2_{\langle \text{RN MUA}|\text{OO EMG}\rangle} > 0$) indicates that the necessary causal conditions were not satisfied, either for a true unidirectional coupling or for a bidirectional association ($D_{12} \neq 0$) between these recordings.

In the second association [$Y_{\text{OO EMG}}(t)$ vs. $X_{\text{IP MUA}}(t)$, blue curves in Fig. 11*A*], the nonlinear associations were only weakly significant in the dynamic correlation range [paired modified Fisher's *z*-test, $H0 = 1$, $P_{\text{Lc}}[\text{w3, w4}] < 0.05$, for the significance of a difference between two measured nonlinear correlation coefficients; mean ± SE, $\eta 3_{\max\langle \text{OO EMG}|\text{IP MUA}\rangle} = 0.573 \pm 0.051$ and $\eta 4_{\max\langle \text{IP MUA}|\text{OO EMG}\rangle} = 0.545 \pm 0.037$]. However, moderate and low nonlinear association index values are not necessarily indicative of an absence of functional relationships between the involved signals. As a result, the information of asymmetry for the maximum values of the nonlinear association indices $[\Delta(\eta 34)^2 = \eta 3^2_{\max\langle \text{OO EMG}|\text{IP MUA}\rangle} - \eta 4^2_{\max\langle \text{IP MUA}|\text{OO EMG}\rangle} \approx 0.031]$ showed a deviation of only 3.1% (i.e., one signal can be explained as a quasi-linear transformation of the other). In the same way, the time delays in the two possible directions of coupling were also positive (mean ± SE, $\tau 3_{\langle \text{OO EMG}|\text{IP MUA}\rangle} = 19.06 \pm 0.15$ ms and $\tau 4_{\langle \text{IP MUA}|\text{OO EMG}\rangle} = 29.04 \pm 0.18$ ms), whereas the relative time delay was negative ($\Delta\tau 34 \approx -9.98$ ms). According to these analyses, the functional interdependence between the recorded signals was quasi-linear and bidirectional [$D_{34} = 0$, $X_{\text{IP MUA}}(t) \rightarrow \text{YES}\ Y_{\text{OO EMG}}(t)$; i.e., the OO EMG response variations can be explained by the preceding red nucleus neuronal activity practically with the same strength that vice versa] during the ninth training session, a result that was also verified for the preceding conditioning sessions (data not shown). In contrast with the first analysis, the bidirectional coupling indicated a feedback relationship between the OO EMG and interpositus neuronal signals [$Y_{\text{OO EMG}}(t)$ and $X_{\text{IP MUA}}(t)$] recorded during the classical conditioning of eyelid responses. These data suggest that instead of one signal exclusively driving the other, each signal [$Y_{\text{OO EMG}}(t)$ and $X_{\text{IP MUA}}(t)$] influences the other.

In the third dynamic association (green curves in Fig. 11*A*), the functional interdependence between the simultaneously recorded signals [$X_{\text{IP MUA}}(t)$ and $X_{\text{RN MUA}}(t)$] was also bidirectional [$D_{56} = 0$, $X_{\text{IP MUA}}(t) \rightarrow \text{YES}\ Y_{\text{RN MUA}}(t)$; i.e., the changes in response of red nucleus neurons can be explained by the preceding interpositus neuronal activity practically with the same strength that vice versa]. The nonlinear associations were only slightly significant in the dynamic correlation range [paired modified Fisher's *z*-test, $H0 = 1$, $P_{\text{Lc}}[\text{w5, w6}] < 0.05$, for the significance of a difference between two measured nonlinear correlation coefficients; means ± SE, $\eta 5_{\max\langle \text{RN MUA}|\text{IP MUA}\rangle} = 0.571 \pm 0.046$ and $\eta 6_{\max\langle \text{IP MUA}|\text{RN MUA}\rangle} = 0.557 \pm 0.019$]. The degree of asymmetry in coupling for the maximum values of the nonlinear association indices $[\ ]\Delta(\eta 56)^2 = \eta 5^2_{\max\langle \text{RN MUA}|\text{IP MUA}\rangle} - \eta 6^2_{\max\langle \text{IP MUA}|\text{RN MUA}\rangle} \approx 0.016$] presented a deviation of only 1.6%. Finally, the time delays in the two possible directions of coupling were also positive (mean ± SE, $\tau 5_{\langle \text{RN MUA}|\text{IP MUA}\rangle} = 16.12 \pm 0.17$ ms and $\tau 6_{\langle \text{IP MUA}|\text{RN MUAG}\rangle} = 24.30 \pm 0.21$ ms), whereas the relative time delay was negative ($\Delta\tau 56 \approx -8.18$ ms).

In summary, the functions w1 and w2 (OO EMG vs. red nucleus MUA coupling and vice versa) for Lurcher data showed significant differences at the asymptotic level of acquisition of the conditioned responses. As a result, the signals $X_{\text{RN MUA}}(t)$ and $Y_{\text{OO EMG}}(t)$ were only reasonably dependent (see Fig. 12*B*) with high values of the association index in the preferential direction of coupling and intermediate values in the opposite direction. Thus the dynamic association was clearly asymmetric (nonlinear relationship) and their positive time delays determined only a spurious unidirectional coupling (see Table 3 for a qualitative report for all the associations from animal model with cerebellar cortical degeneration). In contrast, the functions w3 and w5 for Lurcher data (OO EMG vs. interpositus MUA and red nucleus MUA vs. interpositus MUA, respectively) did not have significant differences—that is, an apparent quasi-symmetric relationship (quasi-linear interdependence) between the $X_{\text{IP MUA}}(t)$ and either $Y_{\text{OO EMG}}(t)$ or $X_{\text{RN MUA}}(t)$, with a clear bidirectional coupling (see Table 3) determined by the positive signs of their time delays. Note that, in these associations the symmetry gains were due to an evident loss of correlation in the preferential direction of coupling [from signal $X_{\text{IP MUA}}(t)$ to either $Y_{\text{OO EMG}}(t)$ or $X_{\text{RN MUA}}(t)$ signals]. According to these results, we can suggest that the high symmetry (low asymmetry between $\eta 3$ and $\eta 4$ association functions with significant differences between w3 and w4 functions,

but without significant differences between w3 and w5 functions; see Tables 2 and 3) in the OO EMG and interpositus MUA coupling is compensating (by modulation of the correlation code) the low symmetry (high asymmetry between $\eta 1$ and $\eta 2$ association functions with significant differences between w1 and w2 functions; see Tables 2 and 3) in the OO EMG and red nucleus MUA coupling. The latter probably caused the high symmetry (low asymmetry between $\eta 5$ and $\eta 6$ association functions with significant differences between w5 and w6 functions, but without significant differences between w5 and w3 functions; see Tables 2 and 3) in the red nucleus MUA and interpositus MUA coupling in Lurcher mice.

DISCUSSION

Contribution of cerebellar structures to the generation of eyelid conditioned responses

The use of mutant and genetically manipulated mice (Chen et al. 1996; Dusart et al. 2006; Kishimoto et al. 2001, 2002; Koekkoek et al. 2003; Lalonde and Strazielle 2007; Porras-García et al. 2005) constitutes a very interesting tool for the study of cerebellar involvement in the acquisition of new motor abilities. Indeed, Lurcher mice present a noticeable ataxic syndrome, as confirmed by their poor performance in various laboratory tasks aimed at quantifying normal motor behavior (Křížková and Vožeh 2004; Porras-García et al. 2005). According to the present results, and in agreement with a previous report (Porras-García et al. 2005), reflexively evoked blinks in Lurcher mice present a longer latency and a smaller amplitude in the late (R2; following Kugelberg 1952) component, compared with littermate controls, with no significant differences for the early (R1) component. This functional difference was not relevant for the acquisition of classically conditioned eyelid responses, since learning curves in Lurcher mice presented values similar to those collected from wild-type animals. Although not checked on this occasion, it has been reported that the amplitude of the learned response in Lurcher mice was significantly lower (Porras-García et al. 2005). Other studies carried out in mGluRδ2 (Kishimoto et al. 2001; Takatsuki et al. 2003), mGluR1 (Kishimoto et al. 2002), and pcd (Chen et al. 1996) mutant mice have reported a decrease in the ability of those mice to acquire conditioned blinks. However, acquisition curves depend on the selected criterion and, as indicated earlier, Lurcher mice present eyelid responses smaller than those of their corresponding controls (see Porras-García et al. 2005). Thus and for the appropriate choice of a comparable criterion, it is always necessary to check the effects of cerebellar lesions not only on reflex blink responses, but also on the kinematics of conditioned responses—that is, differences between learning and performance should always be taken into account (Bracha et al. 2009; Delgado-García and Gruart 2006; Jiménez-Díaz et al. 2004; Van Alphen et al. 2002; Wells and Harvey 1989). Interestingly, following the electrolytic lesion of the interpositus nucleus, the learning curves of both wild-type and Lurcher mice were severely affected. Since the reported lesion significantly reduced reflexively evoked eyeblinks in both groups of animals, the changes in learning could be ascribed to the evident performance deficit. In an experimental attempt to solve this argument between learning and performance, we decided to directly record the neural activity in the interpositus–red nucleus–OO EMG axis. The aim was to record the actual firing responses present in those functional elements during the acquisition process, in the presence (wild-type) or absence (Lurcher) of an overlying cerebellar cortex.

Comparison of the dynamic associations in the "cerebellar–premotor–final motor pathway" network during the classical conditioning in wild-type and Lurcher mice

According to the present results, Lurcher mice do not show significant changes in the temporal orders (relative variations of τi, τj, and $\Delta\tau$ij, where i = 1, 3, 5 and j = i + 1) of coupling between the multiunitary recordings (red nucleus MUA and interpositus MUA) and the OO EMG activity, with respect to data collected from wild-type animals. In all of the dynamic association functions (Figs. 10*A* and 11*A*), the time delays were located to the right of the zero reference point. Thus the absence of cerebellar cortex in the Lurcher mice did not change the causal relationships in the "cerebellar (interpositus MUA)–premotor (red nucleus MUA)–final motor pathway (OO EMG)" network with respect to wild-type data. However, although the relative causality was not affected, the neuronal activities in both red and interpositus nuclei presented a different level of correlation with the conditioned motor response (OO EMG activity), compared with values collected from controls. As a consequence, those variations modified the degree of asymmetry (or symmetry) of the functional coupling among the electrophysiological recordings collected from Lurcher mice (Table 3).

For the dynamic associations between the MUA in the red nucleus and the conditioned response (OO EMG), in the animal model with cerebellar cortical degeneration, a significant gain (≈16.2%, increasing from 6.4% in the wild-type mice to 22.6% in the Lurcher mice) of the asymmetry information of coupling was observed. In contrast, the dynamic associations between the MUA in the cerebellar interpositus nucleus and the conditioned response (OO EMG) showed a significant loss (≈16.8%, decreasing from 19.9% in the wild-type mice to 3.1% in the Lurcher mice) of the asymmetry degree. A similar loss (≈14.1%, decreasing from 15.7% in the wild-type mice to 3.1% in the Lurcher mice) of asymmetry (i.e., a gain in the symmetry and, consequently, a quasi-linear coupling between the recordings) was observed in the dynamic association between MUAs in both red and interpositus nuclei in the Lurcher mice. Furthermore, in the Lurcher mice, the nonlinear association index decreased for the OO EMG versus red nucleus MUA association in the nonpreferential direction of coupling. However, we obtained that for the OO EMG versus interpositus nucleus MUA association, and the red nucleus versus interpositus MUAs coupling, the nonlinear association index decreased in the preferential direction of coupling (Figs. 10*A* and 11*A*). Thus the interpositus nucleus did not directly encode either MUA in the premotor red nucleus or the OO EMG in the final motor pathway of eyelid motor response. Its contribution was only slightly significant in the dynamic correlation range and this regularity in the Lurcher data caused compensation by modulation of the asymmetric degree in the OO EMG versus red nucleus MUA in the nonpreferential direction of coupling. The foregoing allowed us to explain the significant differences between w1 and w2 functions (increase of the asymmetry between $\eta 1$ and $\eta 2$

association functions) and the nonsignificant differences between w3 and w5 functions (decrease of the asymmetry between $\eta 3$ and $\eta 4$ association functions and the same between $\eta 5$ and $\eta 6$ association functions) in the Lurcher data (Figs. 11 and 12*B*, Table 2, Supplemental Fig S4*B*, and Supplemental Table S3).

This increase in the nonlinearity of the coupling between the red nucleus MUA and OO EMG recordings, in association with the decrease in the asymmetry of the coupling between the interpositus nucleus MUA and OO EMG recordings during this associative learning process in the Lurcher mice, would be explained if the cerebellar cortical degeneration induced a reorganization of the relative level of correlation codes of the interpositus and red nuclei neurons to the conditioned response. In wild-type data the cerebellar cortex and olivary system might contribute by maintaining the asymmetric information and the general dynamic control during the learning task (Bracha et al. 2009; D'Angelo et al. 2009; Hong and Optican 2008; Van Der Giessen et al. 2008; Velarde et al. 2004). In the Lurcher mice, the limited contribution of the olivo–cerebellar complex to the correlation code could play an important role in the actual compensatory mechanism (by modulation of the asymmetry degree) of the interpositus and red nucleus neurons during performance of learned movements. It could thus be concluded that in Lurcher mice, the red and interpositus nuclei mutually redistributed their firing rates in the CS–US interval and this reorganization did not affect the causal inferences of the dynamic associations in the "cerebellar (interpositus MUA)–premotor (red nucleus MUA)–final motor pathway (OO EMG)" network, but the variations of the relative correlation codes and the asymmetries of coupling among the electrophysiological recordings were functionally significant. This conclusion further suggests that the adjustment in correlation following Purkinje cell degeneration constitutes an active, compensatory, and measurable response to the degeneration.

Such evidence allowed us to verify in a further species (wild-type and Lurcher mice) our previous results in behaving cats regarding the reinforcing-modulation role of the posterior interpositus nucleus in motor learning (Gruart et al. 2000; Jiménez-Díaz et al. 2004; Sánchez-Campusano et al. 2007, 2009), as well as results collected in rabbits during classical conditioning of the eyeblink nictitating membrane response (Berthier and Moore 1990; Welsh 1992). It could thus be concluded that deep cerebellar nuclear cells (interpositus and dentate nuclei) may be involved more to the modulation and proper performance of ongoing conditioned responses (Sánchez-Campusano et al. 2007) than to their generation and/or initiation and that the firing-movement relationship contains noncausal and nonlinear components (Berthier et al. 1991; Sánchez-Campusano et al. 2009). The present (experimental and analytical) approaches allowed us to show how the red nucleus participates in this modulation process by compensation of the asymmetric information during the performance of the conditioned response. Thus the animal model of cerebellar cortical degeneration (Lurcher mice) was an excellent experimental model to demonstrate the limited participation of the cerebellum in the generation of the conditioned response and the patent participation of the red and interpositus nuclei in its modulation by compensation of their correlation codes during the learning process.

ACKNOWLEDGMENTS

We thank M. Sutil and R. Fernández-Más for technical assistance and R. Churchill for editorial help.

GRANTS

This work was supported by Spanish Ministerio de Educación y Ciencia Grants BFU2007-67173, BFU2008-00899, CVI122, CVI2487, and RD06/0013/0015.

DISCLOSURES

No conflicts of interest, financial or otherwise, are declared by the author(s).

REFERENCES

Aksenova TI, Chibirova OK, Dryga OA, Tetko IV, Benabid A-L, Villa AEP. An unsupervised automatic method for sorting neuronal spike waveforms in awake and freely moving animals. *Methods* 30: 178–187, 2003.

Ansari-Asl K, Senhadji L, Bellanger JJ, Wendling F. Quantitative evaluation of linear and nonlinear methods characterizing interdependencies between brain signals. *Phys Rev E Stat Nonlin Soft Matter Phys* 74: 31916/1178–13, 2006.

Belsley DA, Kuh E, Welsch RE. *Regression Diagnostics: Identifying Influential Data and Sources of Collinearity*. New York: Wiley, 1980.

Bernasconi C, Von Stein A, Chiang C, Konig P. Bidirectional interactions between visual areas in the awake behaving cat. *Neuroreport* 11: 689–692, 2000.

Berthier NE, Barto AG, Moore JW. Linear systems analysis of the relationship between firing of deep cerebellar neurons and the classically conditioned nictitating membrane response in rabbits. *Biol Cybern* 65: 99–105, 1991.

Berthier NE, Moore JW. Activity of deep cerebellar nuclear cells during classical conditioning of nictitating membrane extension in rabbits. *Exp Brain Res* 83: 44–54, 1990.

Boele HJ, Koekkoek SKE, De Zeeuw CI. Cerebellar and extracerebellar involvement in mouse eyeblink conditioning: the ACDC model (Abstract). *Front Cell Neurosci* 3: 19, 2010.

Bracha V, Kolb FP, Irwin KB, Bloedel JR. Inactivation of interposed nuclei in the cat: classically conditioned withdrawal reflexes, voluntary limb movements and the action primitive hypothesis. *Exp Brain Res* 126: 77–92, 1999.

Bracha V, Zbarska S, Parker K, Carrel A, Zenitsky G, Bloedel JR. The cerebellum and eye-blink conditioning: learning versus network performance hypotheses. *Neuroscience* 162: 787–796, 2009.

Brown EN, Kass RE, Mitra PP. Multiple neural spike train data analysis: state-of-the-art and future challenges. *Nat Neurosci* 7: 456–461, 2004.

Cendelín J, Korelusová I, Vožeh F. The effect of repeated rotarod training on motor skills and spatial learning ability in Lurcher mutant mice. *Behav Brain Res* 189: 65–74, 2008.

Cendelín J, Korelusová I, Vožeh F. The effect of cerebellar transplantation and enforced physical activity on motor skills and spatial learning in adult Lurcher mutant mice. *Cerebellum* 8: 35–45, 2009.

Chan HL, Wu T, Lee ST, Fang SC, Chao PK, Lin MA. Classification of neuronal spikes over the reconstructed phase space. *J Neurosci Methods* 168: 203–211, 2008.

Chen L, Bao S, Lockard JM, Kim JK, Thompson RF. Impaired classical eyeblink conditioning in cerebellar-lesioned and Purkinje cell degeneration (pcd) mutant mice. *J Neurosci* 16: 2829–2838, 1996.

Christian KM, Thompson RF. Neural substrates of eyeblink conditioning: acquisition and retention. *Learn Mem* 10: 427–455, 2003.

D'Angelo E, Koekkoek SK, Lombardo P, Solinas S, Ros E, Garrido J, Schonewille M, De Zeeuw CI. Timing in the cerebellum: oscillations and resonance in the granular layer. *Neurosci* 162: 805–815, 2009.

Delgado-García JM, Gruart A. Building new motor responses: eyelid conditioning revisited. *Trends Neurosci* 29: 330–338, 2006.

Domínguez-del-Toro E, Rodríguez-Moreno A, Porras-García E, Sánchez-Campusano R, Blanchard V, Laville M, Bohme GA, Benavides J, Delgado-García JM. An in vitro and in vivo study of early deficits in

associative learning in transgenic mice that over-express a mutant form of human APP associated with Alzheimer's disease. *Eur J Neurosci* 20: 1945–1952, 2004.

Dusart I, Guenet JL, Sotelo C. Purkinje cell death: differences between developmental cell death and neurodegenerative death in mutant mice. *Cerebellum* 5: 163–173, 2006.

Grafen A, Hails R. *Modern Statistics for the Life Sciences.* New York: Oxford Univ. Press, 2002.

Gruart A, Blázquez P, Delgado-García JM. Kinematics of spontaneous, reflex, and conditioned eyelid movements in alert cat. *J Neurophysiol* 74: 226–248, 1995.

Gruart A, Delgado-García JM. Discharge of identified deep cerebellar nuclei neurons related to eye blinks in the alert cat. *Neurosci* 61: 665–681, 1994.

Gruart A, Guillazo-Blanch G, Fernández-Mas R, Jiménez-Díaz L, Delgado-García JM. Cerebellar posterior interpositus nucleus as an enhancer of classically conditioned eyelid responses in alert cats. *J Neurophysiol* 84: 2680–2690, 2000.

Hair JF, Anderson RE, Tatham RL, Black WC. *Multivariate Data Analysis.* Englewood Cliffs, NJ: Prentice Hall, 1998.

Hong S, Optican LM. Interaction between Purkinje cells and inhibitory interneurons may create adjustable output waveforms to generate timed cerebellar output. *PLoS ONE* 3: e2770, 2008.

Jarvis MR, Mitra PP. Sampling properties of the spectrum and coherency in sequences of action potentials. *Neural Comput* 13: 717–749, 2001.

Jiménez-Díaz L, Navarro-López de Dios J, Gruart A, Delgado-García JM. Role of cerebellar interpositus nucleus in the genesis and control of reflex and conditioned eyelid responses. *J Neurosci* 24: 9138–9145, 2004.

Kalitzin SN, Parra J, Velis DN, Lopes da Silva FH. Quantification of unidirectional nonlinear associations between multidimensional signals. *IEEE Trans Biomed Eng* 54: 454–461, 2007.

Kamiński M, Liang H. Causal influence: advances in neurosignal analysis. *Crit Rev Biomed Eng* 33: 347–430, 2005.

Kishimoto Y, Fujimichi R, Araishi K, Kawahara S, Kano M, Aiba A, Kirino Y. mGluR1 in cerebellar Purkinje cells is required for normal association of temporally contiguous stimuli in classical conditioning. *Eur J Neurosci* 16: 2416–2424, 2002.

Kishimoto Y, Kawahara S, Suzuki M, Mori H, Mishina M, Kirino Y. Classical eyeblink conditioning in glutamate receptor subunit delta 2 mutant mice is impaired in the delay paradigm but not in the trace paradigm. *Eur J Neurosci* 13: 1249–1253, 2001.

Koekkoek SKE, Den Ouden WL, Perry G, Highstein SM, De Zeeuw CI. Monitoring kinetic and frequency-domain properties of eyelid responses in mice with magnetic distance measurement technique. *J Neurophysiol* 88: 2124–2133, 2002.

Koekkoek SKE, Hulscher HC, Dortland BR, Hensbroek RA, Elgersma Y, Ruigrok TJH, De Zeeuw CI. Cerebellar LTD and learning dependent timing of conditioned eyelid responses. *Science* 301: 1736–1739, 2003.

Koekkoek SKE, Yamaguchi K, Milojkovic BA, Dortland BR, Ruigrok TJH, Maex R, De Graaf W, Smit AE, VanderWerf F, Bakker CE, Willemsen R, Ikeda T, Kakizawa S, Onodera K, Nelson DL, Mientjes E, Joosten M, De Schutter E, Oostra BA, Ito M, De Zeeuw CI. Deletion of *FMR1* in Purkinje cells enhances parallel fiber LTD, enlarges spines, and attenuates cerebellar eyelid conditioning in fragile X syndrome. *Neuron* 47: 339–352, 2005.

Křížková A, Vožeh F. Development of early motor learning and topical motor skills in a model of cerebellar degeneration. *Behav Brain Res* 150: 65–72, 2004.

Kugelberg E. Facial reflexes. *Brain* 75: 385–396, 1952.

Lalonde R, Strazielle C. Spontaneous and induced mouse mutations with cerebellar dysfunctions: behavior and neurochemistry. *Brain Res* 1140: 51–74, 2007.

Lopes da Silva FH, Pijn JP, Boeijinga P. Interdependence of EEG signals: linear vs. nonlinear associations and the significance of time delays and phase shifts. *Brain Topogr* 2: 9–18, 1989.

Meeren HK, Pijn JP, Luijtelaar EL, Coenen AM, Lopes da Silva FH. Cortical focus drives widespread corticothalamic networks during spontaneous absence seizures in rats. *J Neurosci* 22: 1480–1495, 2002.

Morcuende S, Delgado-García JM, Ugolini G. Neuronal premotor networks involved in eyelid responses: retrograde transneuronal tracing with rabies virus from the orbicularis oculi muscle in the rat. *J Neurosci* 22: 8808–8818, 2002.

Paxinos G, Franklin KBJ. *The Mouse Brain in Stereotaxic Coordinates.* London: Academic Press, 2001.

Pereda E, Quian-Quiroga R, Bhattacharya J. Nonlinear multivariate analysis of neurophysiological signals. *Prog Neurobiol* 77: 1–37, 2005.

Pijn JP, Velis DN, van der Heyden MJ, DeGoede J, van Veelen CW, Lopes da Silva FH. Nonlinear dynamics of epileptic seizures on basis of intracranial EEG recordings. *Brain Topogr* 9: 249–270, 1997.

Porras-García E, Cendelín J, Domínguez-del-Toro E, Vožeh F, Delgado-García JM. Purkinje cell loss affects differentially the execution, acquisition and prepulse inhibition of skeletal and facial motor responses in Lurcher mice. *Eur J Neurosci* 21: 979–988, 2005.

Sakamoto T, Endo S. $GABA_A$ receptors in deep cerebellar nuclei play important roles in mouse eyeblink conditioning. *Brain Res* 1230: 125–137, 2008.

Sánchez-Campusano R, Gruart A, Delgado-García JM. The cerebellar interpositus nucleus and the dynamic control of learned motor responses. *J Neurosci* 27: 6620–6632, 2007.

Sánchez-Campusano R, Gruart A, Delgado-García JM. Dynamic associations in the cerebellar–motoneuron network during motor learning. *J Neurosci* 29: 10750–10763, 2009.

Svensson P, Ivarsson M, Hesslow G. Effect of varying the intensity and train frequency of forelimb and cerebellar mossy fiber conditioned stimuli on the latency of conditioned eye-blink responses in decerebrate ferrets. *Learn Mem* 4: 105–115, 1997.

Takatsuki K, Kawahara S, Kotani S, Fukunaga S, Mori H, Mishina M, Kirino Y. The hippocampus plays an important role in eyeblink conditioning with a short trace interval in glutamate receptor subunit δ2 mutant mice. *J Neurosci* 23: 17–22, 2003.

Van Alphen AM, Schepers T, Luo C, De Zeeuw CI. Motor performance and motor learning in Lurcher mice. *Ann NY Acad Sci* 978: 413–424, 2002.

Van Der Giessen RS, Koekkoek SK, van Dorp S, De Gruijl JR, Cupido A, Khosrovani S, Dortland B, Wellershaus K, Degen J, Deuchars J, Fuchs EC, Monyer H, Willecke K, De Jeu MTG, De Zeeuw CI. Role of olivary electrical coupling in cerebellar motor learning. *Neuron* 58: 599–612, 2008.

Velarde MG, Nekorkin VI, Makarov VA, Makarenko VI, Llinás RR. Clustering behavior in a three-layer system mimicking olivo-cerebellar dynamics. *Neural Networks* 17: 191–203, 2004.

Vogel MW, Caston J, Yuzaki M, Mariani J. The Lurcher mouse: fresh insights from an old mutant. *Brain Res* 1140: 4–18, 2007.

Welsh JP. Changes in the motor pattern of learned and unlearned responses following cerebellar lesions: a kinematic analysis of the nictitating membrane reflex. *Neuroscience* 47: 1–19, 1992.

Welsh JP, Harvey JA. Cerebellar lesions and the nictitating membrane reflex: performance deficits of the conditioned and unconditioned response. *J Neurosci* 9: 299–311, 1989.

Wendling F, Bartolomei F, Bellanger JJ, Chauvel P. Interpretation of interdependencies in epileptic signals using a macroscopic physiological model of the EEG. *Clin Neurophysiol* 112: 1201–1218, 2001.

Witte H, Unqureanu M, Ligges C, Hemmelmann D, Wüstenberg T, Reichenbach J, Astolfi L, Babiloni F, Leistritz L. Signal informatics as an advanced integrative concept in the framework of medical informatics. New trends demonstrated by examples derived from neuroscience. *Methods Inf Med* 48: 18–28, 2009.

Yeo CH, Hardiman MJ, Glickstein M. Classical conditioning of the nictitating membrane response of the rabbit. I. Lesions of the cerebellar nuclei. *Exp Brain Res* 60: 87–98, 1985.

Yuzaki M. The delta2 glutamate receptor: a key molecule controlling synaptic plasticity and structure in Purkinje cells. *Cerebellum* 3: 89–93, 2004.